Journal of *Marine Science and Engineering*

MDPI

Article

Integrated Approach to Ship Electrification Using Fuel Cells and an Ammonia Decomposition System

Onur Yuksel [1,2,*], Eduardo Blanco-Davis [1], David Hitchmough [1], G Viknash Shagar [1], Andrew Spiteri [1], Maria Carmela Di Piazza [3], Marcello Pucci [3], Nikolaos Tsoulakos [4], Milad Armin [5] and Jin Wang [1]

1 Liverpool Logistics Offshore and Marine Research Institute (LOOM), School of Engineering, Liverpool John Moores University, Byrom Street, Liverpool L3 3AF, UK; e.e.blancodavis@ljmu.ac.uk (E.B.-D.); d.m.hitchmough@ljmu.ac.uk (D.H.); g.v.shagar@ljmu.ac.uk (G.V.S.); spiteri.andrew94@gmail.com (A.S.); j.wang@ljmu.ac.uk (J.W.)
2 Marine Engineering Department, Maritime Faculty, Zonguldak Bülent Ecevit University, Kepez District, Hacı Eyüp Street, No. 1, 67300 Zonguldak, Türkiye
3 National Research Council of Italy (CNR), Institute of Marine Engineering (INM), via Ugo La Malfa 153, 90146 Palermo, Italy; mariacarmela.dipiazza@cnr.it (M.C.D.P.); marcello.pucci@cnr.it (M.P.)
4 Laskaridis Shipping Co., Ltd., 5 Xenias Str. and Ch. Trikoupi, 14562 Athens, Greece; tsoulakos@laskaridis.com
5 Enki Marine Technology Consultancy, Unit 5 Reliance House, 20 Water Street, Liverpool L2 8AA, UK; m.armin@enkimarine.co.uk
* Correspondence: o.yuksel@ljmu.ac.uk

Abstract: This study investigates the environmental and economic performance of integrating a proton exchange membrane fuel cell, battery systems, and an organic Rankine cycle-based waste heat recovery system for ship electrification. The analysis examines an onboard ammonia decomposition system for hydrogen production and ammonia production pathways. Additionally, the study benchmarks the effectiveness of onboard ammonia decomposition against green hydrogen bunkering scenarios (H_2-BS). The analysis is based on data collected over two years from a bulk carrier provided by Laskaridis Shipping Co., Ltd. The environmental analysis includes well-to-wake emissions calculations. At the same time, economic performance is assessed through levelised cost of energy (LCOE) computations for 2025 and 2040, factoring in different fuel and carbon price scenarios. Consequently, the analysis utilises the Complex Proportional Assessment method to compare configurations featuring various ammonia production pathways across economic cases. The results indicate that green and pink ammonia feedstocks achieve maximum equivalent carbon dioxide reductions in the electrification plant of up to 47.28% and 48.47%, respectively, compared to H_2-BS and 95.56% and 95.66% compared to the base scenario. Ammonia decomposition systems prove more economically viable than H_2-BS due to lower storage and fuel costs, leading to competitive LCOE values that improve under higher carbon pricing scenarios.

Keywords: maritime decarbonisation; ship electrification; ammonia (NH_3) decomposition; hydrogen (H_2); proton exchange membrane fuel cell (PEMFC); levelised cost of energy (LCOE); multi-criteria decision-making (MCDM)

Academic Editors: Yulong Ji and Daan Cui

Received: 14 April 2025
Revised: 13 May 2025
Accepted: 14 May 2025
Published: 18 May 2025

Citation: Yuksel, O.; Blanco-Davis, E.; Hitchmough, D.; Shagar, G.V.; Spiteri, A.; Di Piazza, M.C.; Pucci, M.; Tsoulakos, N.; Armin, M.; Wang, J. Integrated Approach to Ship Electrification Using Fuel Cells and an Ammonia Decomposition System. *J. Mar. Sci. Eng.* **2025**, *13*, 977. https://doi.org/10.3390/jmse13050977

1. Introduction

Maritime transportation has been crucial to carrying cargo and passengers for decades, and its worldwide capacity has increased drastically recently [1]. The increased fossil fuel usage for marine vessels' propulsion and electricity generation significantly contributes to global warming [2]. The International Maritime Organization (IMO) has instituted regulations designed to advance sustainable shipping practices while establishing ambitious

targets for the reduction of waterborne emissions [3]. The short-term objectives for 2030 include a 40% reduction in carbon dioxide (CO_2) emissions and a 20% decrease in overall greenhouse gases (GHG), with the intention of achieving 30%. Additionally, there is a target for 5% utilisation of zero-emission fuels, striving for 10%. In the midterm, the goals are to achieve a 70% reduction in total GHG emissions, with aspirations for an 80% decrease, ultimately leading to net-zero emissions by 2050 [4].

In recent years, ammonia (NH_3) and NH_3-involved compounds have emerged as a popular zero-carbon alternative fuel for marine vessels [5,6]. Its use in marine diesel engines (MDEs) and as a hydrogen (H_2) carrier has been a timely topic for the maritime sector [6]. NH_3 contains 17.6 wt.% H_2, and it is a gas at room temperature and pressure, becoming liquid at 263 K or 1000 kPa [7]. Its well-established industrial production, primarily for fertiliser, makes it a cost-effective option [8].

NH_3 has been prominent as an H_2 carrier in maritime applications, mainly due to the technical and safety challenges associated with storing H_2 onboard ships. H_2 storage is complicated by its low volumetric energy density and high flammability, which demand either cryogenic conditions for liquefaction or high-pressure containment systems. These requirements introduce significant engineering and safety concerns on marine vessels [9].

The most significant disadvantage of NH_3 is its toxicity and dangerous nature for human health. Considerable health consequences, including blindness, lung damage, brain damage, and maybe even death, can arise from exposure to elevated levels of NH_3 in the air [10,11]. Consequently, NH_3 leaks can quickly escalate into a significant risk to the accommodations and crew members on board [12].

Despite its high toxicity and corrosiveness [13], NH_3 is an effective H_2 carrier [6]. However, its properties require an improved design meeting specific codes and rules, in addition to increased requirements [12]. The production methodology of NH_3 is also a significant subject since green (renewables-sourced) or pink (nuclear-sourced) NH_3 has been required to meet the net-zero targets. The clean NH_3 capacity and prices to meet the demand of the maritime sector have been a remarkable challenge for the utilisation in shipping operations [14]. Compared to the bunkering, storage, and transfer operations for H_2, producing it from NH_3 would be much more cost-effective and applicable [15].

1.1. Literature Review

Several research papers about the onboard utilisation of NH_3-based systems to generate H_2 on marine vessels have been published. Over the past few years, the utilisation of NH_3 as an H_2 carrier or as a direct fuel for fuel cells (FCs) in marine applications has attained prominence, driven by the IMO's targets for maritime decarbonisation.

Boggs and Botte [16] applied NH_3 electrolysis with an NH_3 electrolytic cell to generate H_2 onboard vessels in a Proton Exchange Membrane Fuel Cell (PEMFC). H_2 can be extracted from NH_3 via electrolysis, which theoretically requires 95% less energy than water electrolysis. Specifically, NH_3 electrolysis consumed 1.55 Whg^{-1} of H_2, whereas water electrolysis requires 33 Whg^{-1} of H_2.

Wang et al. [17] demonstrated the combined usage of NH_3 auto-thermal reforming and selective NH_3 oxidation to produce H_2 by utilising the waste heat in the exhaust gas of diesel engines. H_2 production at 2.5–3.2 L/min was achieved when the NH_3 was supplied steadily at a 3 L/min flow rate.

McKinlay et al. [18] presented a dynamic simulation of NH_3 decomposition to produce H_2 for PEMFCs on marine vessels. The analysis included a detailed assessment of NH_3 demand, revealing that the reference cargo ship would require 150 t of NH_3 per voyage, necessitating a 586 m^3 storage tank.

Ye et al. [19] compared conventional diesel engines with FC propulsion systems using NH_3 and H_2 as fuels for a small ship working as a sea taxi. The storage options of H_2 were evaluated while the presentation of an NH_3 cracking system was ensured in the study. The FC options met the demand of the vessel overall with significant equivalent CO_2 (CO_{2e}) reduction ratios.

Zhu et al. [20] compared methanol and NH_3 as H_2 sources using the life cycle approach, using commercial software. Methanol and NH_3 were evaluated as H_2 carriers compared to coal, natural gas, and renewable energy sources. The solar energy-based NH_3 plant produced the lowest CO_{2e} per MJ at 43.9 g.

Spatolisano et al. [21] assessed the potential of NH_3 as a zero-carbon H_2 carrier, analysed the maritime transportation of feedstocks and products, and evaluated the maturity of decomposing technologies for the industry.

Duong et al. [22] presented an innovative multigeneration system that utilises NH_3 as the primary fuel for marine applications. The integration of various components, including PEMFC, solid-oxide FC (SOFC), gas turbines, and waste heat recovery systems (WHRSs) based on diverse thermodynamic cycles, was ensured. The analysis revealed an energy efficiency of 60.69% and an exergy efficiency of 57.50%, with waste heat recovery contributing 1634.46 kW, which accounts for 30.07% of the total power output.

Restelli et al. [23] performed a comprehensive thermo-economic assessment of NH_3 as a green H_2 source onboard ships. The transport cost for the industrial application was between 5.49 and 6.34 EUR/kg, whereas for the mobility end use, it varied between 6.80 and 12.22 EUR/kg.

Di Micco et al. [24] investigated the design and viability of NH_3-based propulsion systems for maritime applications, focusing on two FC technologies: PEMFC and SOFC. The findings revealed that implementing these NH_3 systems increases weight and volume, decreasing cargo capacity by 3.3% to 4.8%.

Duong et al. [25] examined the techno-economic feasibility of a direct NH_3 SOFC system, enhanced by a gas turbine and integrated with a multi-generation framework that includes various energy recovery systems. Key findings indicated that the levelised cost of energy (LCOE) ranges from USD 0.482 to USD 0.554 per kWh, with a variation of about 6.2%. At the same time, the discounted payback period for unsubsidised and subsidised scenarios falls between 6.7 and 9.5 years.

Research on NH_3 utilisation for H_2 production in marine vessels can be broadly categorised into electrolysis-based, thermo-chemical, and system-integrated approaches. Electrolytic systems highlighted the energy efficiency potential of NH_3 electrolysis compared to water electrolysis [16]. Thermo-chemical methods, including auto-thermal reforming [17,18], demonstrated effective H_2 generation using onboard waste heat, though storage and logistics remain challenging.

Integrated system designs have taken a broader view of NH_3 as a fuel or carrier, balancing efficiency, emissions, and cost. Studies comparing NH_3-based systems to conventional marine fuels and H_2 alternative carriers, such as methanol, demonstrated that NH_3 frequently emerges as a lower-emission option when renewable sources are used for NH_3 production [19,20]. Techno-economic [23,25] and system-level assessments [21,22] have shown promising efficiencies and payback periods but have also highlighted concerns regarding volume, weight, and infrastructure demands [24].

In summary, NH_3 is a technically viable H_2 source and direct fuel, offering substantial emission reduction potential, especially when integrated into hybrid or WHRSs. Economic feasibility varies, with performance and system complexity depending heavily on technology choice and operating conditions.

Various research papers have focused on the PEMFC applications on ships apart from NH_3 usage, exploring their potential to enhance energy efficiency, reduce emissions, and improve overall performance in maritime operations.

Sarı et al. [26] established a "Reference Energy System" for a chemical tanker to analyse energy flow from various sources. It evaluated a baseline scenario and introduced two alternatives, including one focused on H_2 PEMFCs. The findings indicated that H_2 PEMFCs can achieve a 60% reduction in carbon emissions compared to diesel generators as a primary propulsion system.

Vieira et al. [27] determined the best configuration for a ship's power system, integrating FCs and batteries, considering battery cycles. The focus was on a retrofitted platform supply vessel with its original generators and additional FCs and batteries. Simulations using commercial software showed that the optimal setup, main and auxiliary generators, a 3119-kW lithium nickel manganese cobalt battery, a 250 kW PEMFC, and 581 kg of H_2 achieved a 10.69% reduction in CO_2 emissions.

Bang et al. [28] examined methane (CH_4) with PEMFCs for their performance and cost advantages over hydrogen. CH_4 was reformed using steam reforming and evaluated through five gas treatment systems. The results showed that combining water–gas shift and partial oxidation reforming keeps carbon monoxide below 10 ppm and prevents CH_4 in the exhaust.

Bagherabadi et al. [29] developed a model for a marine power system using PEMFCs and batteries. It validated the model against a 500 kW PEMFC and demonstrated its effectiveness for performance analysis and control design. The model supported flexibility in configuration and could assess various manoeuvring scenarios.

Lee et al. [30] introduced a PEMFC system combined with an organic Rankine cycle (ORC) that utilises cold exergy from liquid H_2 and waste heat from the PEMFC for marine applications. Findings indicated that the system can produce an additional 221 kW of power, with energy and exergy efficiencies of 40.45% and 43.52%, respectively. Economic analysis suggests a payback period of 11.2 years and a net present value of USD 295,268, demonstrating the system's potential viability.

Wang et al. [31] assessed FC technologies for ship power, focusing on energy efficiency and environmental impact. Low-temperature PEMFCs emerged as the most viable option for sustainable propulsion, with the lowest Energy Efficiency Design Index value at 10.05 g CO_2/t-km.

Penga et al. [32] explored the potential of hybrid systems combining PEMFCs and battery packs as a cleaner alternative to diesel propulsion for marine vessels. A numerical model was developed to optimise a hybrid power system for a specific route, featuring a 300 kWe PEMFC stack and a 424-kWh battery. The results demonstrated that this new system significantly reduced emissions, requiring only 284.7 kg of H_2 compared to 1524 kg of diesel previously consumed.

Yuksel et al. [33] evaluated the integration of various FC technologies with battery storage systems and WHRS for retrofitting marine electricity generation plants. The study employed mathematical modelling and real-time operational data from a Kamsarmax bulk carrier. The analysis showed that hybrid configurations combining PEMFC and SOFC, powered by liquefied green H_2, can reduce well-to-wake equivalent CO_2 emissions from the ship's electrification system by up to 91.79%.

Aziz et al. [34] presented a coordinated control strategy for a hybrid shipboard power system using PEMFCS and batteries. The strategy improved operational efficiency and stabilised power during load changes, achieving a 14.16% increase in system efficiency over traditional methods while maintaining stable voltage tracking.

PEMFCs have received considerable attention for marine decarbonisation, with studies focusing on propulsion replacement, hybridisation, and system optimisation. Initial work [18,26,27] showed that replacing diesel generators with PEMFCs could significantly reduce emissions. Hybrid configurations combining PEMFCs with batteries or other FCs enhanced operational flexibility and emission reduction outcomes [32,33].

Performance modelling and control strategies [29,34] supported system adaptability and efficiency under variable marine conditions. Integration with WHRSs [30] and comparative assessments of PEMFCs against other FC types [31] further confirmed their strong potential in meeting environmental and regulatory targets. Overall, PEMFCs are a well-supported and adaptable low-emission option for marine applications, especially when deployed in hybrid systems or with energy recovery enhancements.

The literature review on PEMFC and NH_3 utilisation in marine vessels reveals a significant surge in research publications in recent years, driven by IMO decarbonisation objectives and growing environmental awareness. NH_3 evaluations as a fuel in power systems have focused on economic and environmental performance.

The studies investigated onboard H_2 production from NH_3 decomposition and evaluated the financial performance, required NH_3 capacity, and ecological benefits. The presented designs have been proposed as a concept for the propulsion system. A gap in the literature has been identified regarding the integrated design evaluation of onboard NH_3 cracking systems and FCs for marine electricity generation plants. The existing literature has been notably deficient in comprehensive analyses that integrate well-to-wake environmental evaluations alongside assessments of economic factors and design requirements for the combined configuration of an integrated NH_3 decomposer and H_2 PEMFC, battery, and WHRS.

1.2. Objectives, Motivation and Novelty

This study presents a comparative analysis of conventional marine diesel generators (D/Gs) utilising heavy fuel oil (HFO), with FCs that employ green H_2 bunkering and NH_3 decomposition systems for onboard H_2 production derived from diverse NH_3 production pathways. Previous research conducted by the authors of [33] evaluated the potential of liquefied natural gas (LNG) reform for H_2 production in FCs, alongside the performance of FCs utilising green H_2 bunkering. The top-ranked configurations utilising green H_2 bunkering from the prior study [33] were employed in this analysis.

This research aims to present an integrated design involving the onboard H_2 production and PEMFC/battery/WHRS hybrid configuration to meet the electricity demand of a Kamsarmax bulk carrier. The analysis has been performed using a robust system for real-time data collection. The feasibility of the proposed hybrid electrification system's economic and environmental performance has been assessed. The financial viability and bunkering challenges of H_2 systems have rendered them unfeasible for current vessels. The study's objective is to reduce fuel costs, increase fuel availability, and thereby enhance the economic performance of H_2 configurations by implementing NH_3-craking systems for the ships.

The upstream (well-to-tank) emissions arising from H_2 generation concerning the NH_3 production methodology and operational emission reductions have been examined to ascertain whether this configuration can serve as a viable option for meeting forthcoming decarbonisation targets. The tank capacities have been identified to illustrate the implementation's specific design and operational challenges. This article distinguishes itself from existing literature by presenting a comprehensive design structure that encompasses both H_2 production and consumption to address the electricity demands of a commercial marine vessel. The system's operational performance was evaluated, and the various NH_3

production methodologies were analysed across different economic projection scenarios using a multi-criteria decision-making (MCDM) algorithm. This paper's innovative aspect lies in integrating a streamlined well-to-wake environmental approach with a multi-criteria decision-making (MCDM) framework for the onboard NH_3 decomposition system. This framework is designed for PEMFC/battery/WHRS configurations within the ship electrification system, accompanied by a discussion of its merits and disadvantages. The thorough investigation of various facets of the system contributes to the existing literature while acting as a significant resource for ship owners, managers, and designers to identify the decarbonisation pathway for their fleets.

2. Materials and Methods

This section provides an overview of the analytical framework and context underlying the research findings, detailing the description of the system utilised in the study. The case study focuses on the Kamsarmax bulk carrier M/V KASTOR, operated by Laskaridis Shipping Co. Ltd. (Athens, Greece) built in 2020, the vessel has a deadweight of 80,996 tonnes and an overall length of 229 metres. Its propulsion system features a HYUNDAI 6S60ME-C8.5 (Ulsan, South Korea) engine with a maximum power output of 9930 kW. The ship also includes an electrification plant comprising three YANMAR 6EY22LW D/Gs (Almere, The Netherlands) operating HFOs, each with a terminal power capacity of 720 kW. Ship particulars and sample data are provided in Yuksel et al. [33].

A bulk carrier without cargo handling gear (gearless bulk carrier) was selected for this study due to its structural potential and further suitability for integrating alternative energy systems, such as photovoltaic (PV) panels or wind turbines, given the available deck space and minimal obstructions. Additionally, these vessels typically exhibit a more stable electrical load profile during port operations, which supports consistent performance evaluation of onboard energy systems. The selection was also driven by the availability of high-quality, long-term sensor data, essential for robust analysis and validation of the proposed methods. Figure 1 demonstrates the application process of the techniques used in the study.

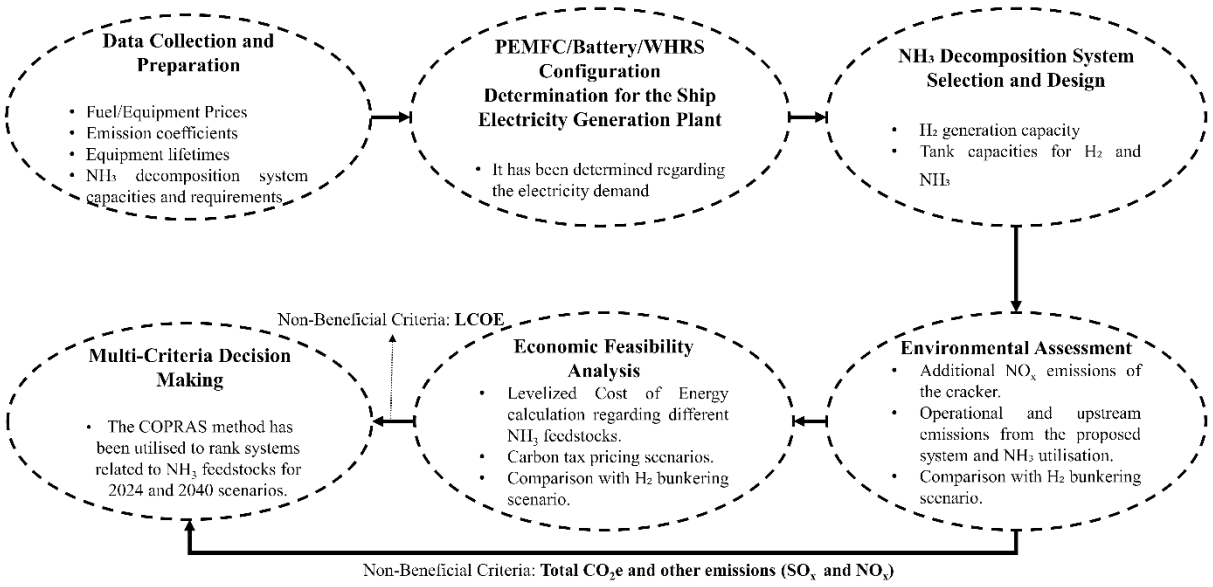

Figure 1. Methodology flowchart.

A data acquisition system was implemented to reliably gather information from sensors and control mechanisms on the case study ship. This system functions through a wireless network, facilitating efficient data collection and monitoring. It has been certified

by Bureau Veritas and complies with maritime safety and operational standards. Major components include the Quax 8S Node, which records voyage-specific metrics such as vessel speed and navigation information; the Quax G Node, which tracks the MDEs' performance; and the Quax S Node, which captures data on flow and revolutions to enhance overall monitoring abilities [35].

The data acquisition period spanned from 1 February 2021 to 10 February 2023. After preprocessing, the dataset was refined to comprise 1,003,490 entries, representing 1.96 years of operational metrics. The collected parameters included measures involving fuel flow, temperature, density, and engine powers, complemented by analyses of electrical load and exhaust data. Furthermore, details related to FC/battery curves, converter voltage, and conversion efficiencies were sourced from the literature and commercial system datasheets.

In the initial stage of the analysis, data on prices, emission coefficients, and properties of the NH_3 cracker were collected. The two PEMFC/battery/WHRS configurations for the marine electricity generation unit were proposed. Subsequently, the design of the NH_3 decomposition system, including the tank and production capacity for H_2, was determined.

The environmental performance of the cracker-involved operations was assessed, considering nitrous oxide (NO_x) emissions from NH_3 combustion and the sulphur oxides (SO_x) and CO_{2e} resulting from the NH_3 production methodology. System economic viability was evaluated by calculating the LCOE for 2025 and 2040 using different colour-coded NH_3 as the feedstock. This financial performance was compared with the green H_2 bunkering scenarios (H_2-BS). The outcomes of these analyses were combined in an MCDM analysis, and the configurations were ranked regarding the NH_3 colour codes.

The integration of the PEMFC/battery/WHRS system into the ship electrification plant was achieved using a simulation created in the Python 3.11 programming environment. It benchmarks the hybrid systems' emission reductions against conventional diesel engines.

The simulation workflow begins with importing required libraries and reading input data. Initial parameters for the hybrid system are defined, and writable lists for logging results are prepared. The algorithm first checks whether the WHRS can generate power based on the main engine (M/E) load. If so, it interpolates the exhaust flow and temperature according to the engine power, then calculates the power generation from the ORC-based WHRS. If not, the WHRS power supply is set to zero. The number of working FCs and D/Gs (if needed) and battery support, including charging and discharging, are determined depending on the power demand. As described above, the hierarchy in PEMFC/battery/WHRS hybrid configurations begins with WHRS and prioritises the PEMFCs. If the required power is within the capacity of the PEMFCs, the FC plant solely meets the load, and the number of active FCs is determined based on the demanded power. The PEMFC H_2 consumption is calculated based on the power–H_2 curves provided by the manufacturer [36]. If the required power exceeds the capacity of the PEMFC plant, the batteries are activated. However, the necessary charging power is added to the required grid power if the batteries need to be charged. Battery charging and discharging operations are determined by assessing the state-of-charge (SoC). Additionally, batteries are used to compensate for instantaneous load demands. If the PEMFC/battery/WHRS plant cannot meet the required power, D/Gs are utilised. The required D/G power is determined by subtracting the required total power from the available PEMFC/battery/WHRS supply. Then, depending on the required D/G power, the specific fuel consumption (SFC) is interpolated, and fuel consumption is calculated. Subsequently, the model computes the utilisation times of each equipment, fuel consumption, and emissions for the PEMFC/battery/WHRS hybrid configurations. Finally, the results are logged, structured into data frames, and exported to spreadsheets for further analysis. The algorithmic framework, which visually elucidates the processes, is presented in Appendix A. The energy management strategy

deciding the hierarchy between power equipment is detailed in a simplified format in Appendix B. Table 1 indicates the analysed configurations.

Table 1. Configurations analysed in the case study.

Case	DGs	PEMFCs	Battery Capacity	WHRS
Base	3 × 720 kW	N/A	N/A	N/A
C1	1 × 720 kW	4 × 200 kW	443 kWh	ORC (Average: 197.01 kW)
C2	2 × 720 kW	2 × 200 kW	123 kWh	ORC (Average: 197.01 kW)

The selection of FC types and sizes in this study was based on a comprehensive prior analysis ranking configurations by performance and size [33]. The chosen commercially available FCs align with the vessel's load profile, which ranges from 200 kW to 800 kW per generator (see Figure 2 given in Yuksel et al. [33]), with a critical threshold power of 400 kW. Thus, the selected FC sizes are positioned either in the middle of this range (C2) or fully satisfy the requirements (C1) within this range to meet the specified power output.

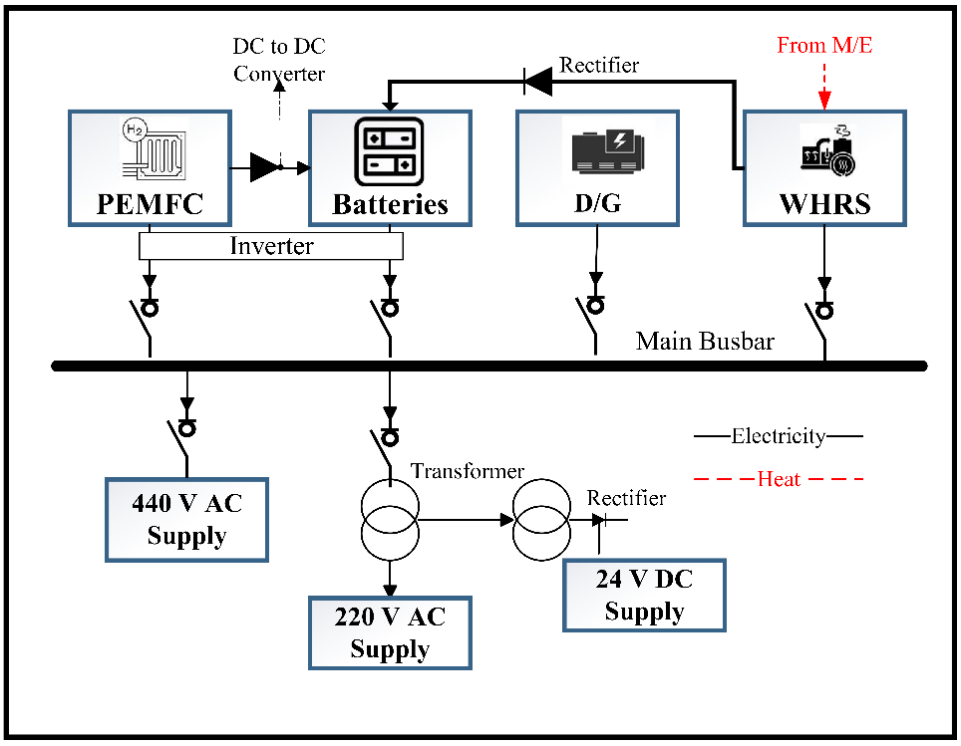

Figure 2. The general system scheme of the investigated hybrid configurations.

Battery sizes were adjusted according to FC sizes and the available average power from the ORC. In the context of the hybrid system, the battery sizes were increased based on the number of generators' loads that needed to be met by the hybrid configuration. The dimensions of the batteries were determined to ensure that, after the FCs and WHRS fulfil the load profile requirements, any remaining demand can be adequately addressed by the batteries during emergency situations. These batteries can support the system for a minimum of one hour and, in certain cases, can provide extended support at a slower discharge rate, thereby enhancing overall system reliability.

This analysis examines two distinct hybrid designs. C1 features a larger FC system with an enhanced battery capacity that can support the load of two generators. This setup comprises four FC units, each rated at 800 kW, supplemented by a WHRS providing

average 197.01 kW and a battery storage capacity of 443 kWh. Together, this configuration effectively meets the combined load of the two generators, totalling 1440 kW.

Configuration C2 integrates an FC, battery, and WHRS to support a single generator's load of 720 kW. In this setup, two FCs share the load of 400 kW, while the WHRS consistently contributes an average additional 197.01 kW during navigation. The battery system supplies the remaining power requirements. It is important to note that the WHRS has a capacity of up to 449.47 kW at full ME load, equivalent to 354.41 kW at 85% ME load. These configurations were the most prominent in the benchmarking against other FC types and sizes within the electrification plant of the case study vessel, as indicated in the study of Yuksel et al. [33]. Figure 2 illustrates the PEMFC/battery/WHRS integrated system scheme in the marine power distribution system.

The batteries are charged by the WHRS utilising the exhaust waste heat from the M/E, in conjunction with PEMFCs, as illustrated in Figure 2. The direct current (DC) of PEMFCs and batteries is inverted to alternating current (AC) before being given to the grid. The ship electrification components' specifications and model details were provided in Yuksel and Koseoglu [37].

2.1. Ammonia Decomposition System

NH_3 cracking, or decomposition, generates H_2 from NH_3 over a catalyst at normal pressures and high temperatures. Without a catalyst, thermal processes that facilitate the NH_3 decomposition typically commence at temperatures exceeding 773 K [38]. Equation (1) indicates the endothermic reaction of NH_3 decomposition [38].

$$2NH_3 \rightleftharpoons 3H_2 + N_2 \; \Delta H_0 = 92.44 \text{ kJ/mol.} \quad (1)$$

In contrast, the presence of a catalyst allows for catalytic cracking to predominantly occur at temperatures below 698 K, achieving an efficiency rate of approximately 98–99% [15,39]. The key factor is the high cracking purity of H_2 (99.9%) since the toxic and corrosive properties of NH_3 can harm the FC systems [38].

Nickel-based catalysts (e.g., Ni/Al_2O_3, Ni/MgO) are among the most widely studied and commercially used due to their cost-effectiveness and reasonable activity, particularly at temperatures above 650 K. These catalysts typically operate with a space velocity of 3000–10,000 h^{-1} and exhibit a deactivation rate influenced by sintering and nitrogen poisoning. In contrast, ruthenium-based catalysts (e.g., Ru/Al_2O_3, Ru/CeO_2) have demonstrated superior activity at lower temperatures (as low as 550–600 K), often achieving near-complete NH_3 conversion at lower residence times and with enhanced thermal stability over prolonged operation [40].

The reactor model developed by Devkota et al. [41] in the Aspen Plus V1.2. and the cracker of Crystec [42] was used in the analysis. The feed NH_3 at 96.3 kg/h capacity, having 298 K and 10 bars, was utilised in the reactor [42]. The reactor model was validated against the experimental and simulated results reported by Devkota et al. [41], with key performance metrics such as NH_3 conversion and reactor outlet temperature aligning within a ±5% margin. The PSA unit performance was also cross-referenced with industrial data from Crystec [42], ensuring technical feasibility and scale relevance. Figure 3 indicates the simplified NH_3 cracker system scheme.

The required heat was met by the combustion of NH_3, which was 9% of the feedstock. The unused NH_3 was mixed with new fuel and air and introduced into the boiler via a pre-heater. A two-bed Temperature Swing Adsorption (TSA) unit separated the remaining NH_3 from the degraded H_2 and nitrogen gas mixture. The waste heat was extracted from the product and flue gas streams using the air–fuel mixture. Ultimately, more than 99.999% pure H_2 at 16.7 kg/h capacity can be produced with a NO_x emission generation

at 0.021 kg-NH_3/kg-H_2 by recirculating the flue gas via an eight-step, four-bed Pressure Swing Adsorption (PSA) machine with two pressure equalisations [15,41,42].

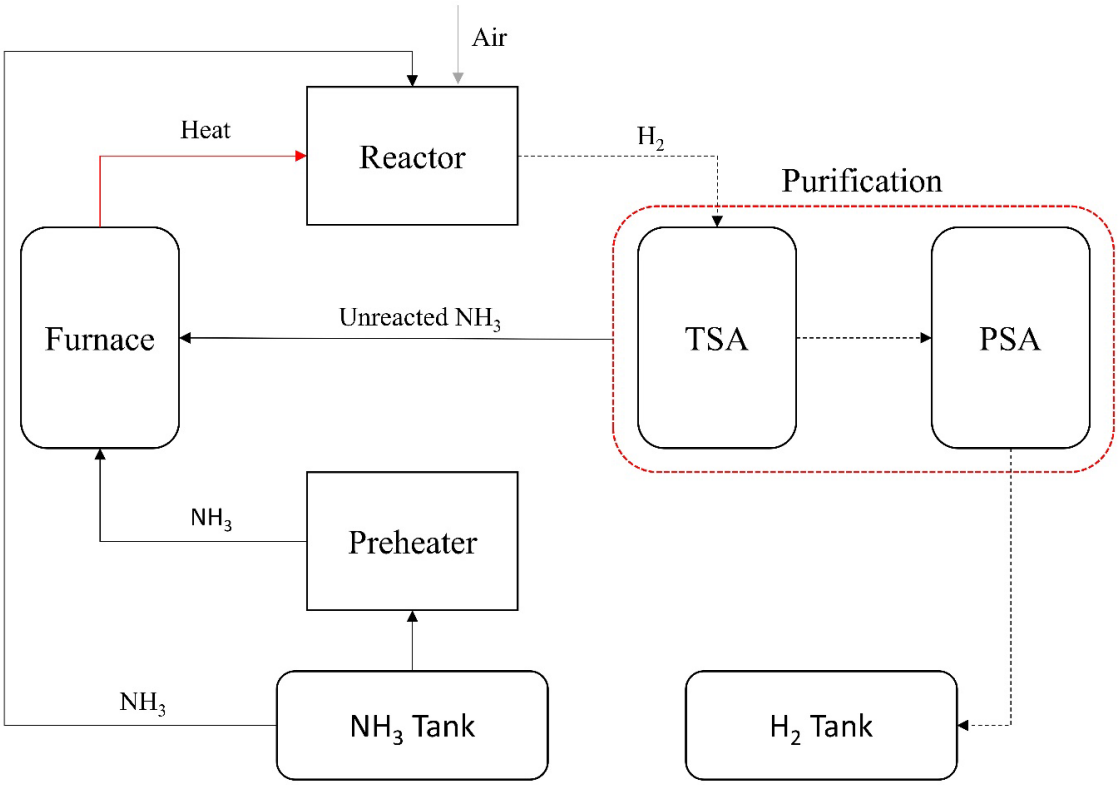

Figure 3. Basic schematic of NH_3 decomposition unit (adapted from [15,41,42]).

The reactor configuration typically involves a packed-bed tubular geometry with internal heating or external jacketed systems to compensate for the endothermic nature of the reaction. Maintaining a uniform temperature distribution in this configuration is critical, as local hot spots may lead to catalyst degradation or uneven NH_3 conversion profiles. Catalyst loading, bed porosity, and tube dimensions are optimised to ensure efficient mass and heat transfer throughout the reactor volume [40,41].

2.2. Ammonia Colour Coldes

The Haber–Bosch process is one of the methods to produce NH_3 by combining nitrogen and H_2 through a thermocatalytic reaction [43]. When the manufacturing was performed using natural gas via steam-methane reforming (SMR), the NH_3 was labelled as "Grey", and the process was assumed to emit 1.88 t-CO_{2e}/t-NH_3 in this study. "Blue NH_3" manufacturing includes a carbon capture system in the plant and reduces emissions to 1.23 t-CO_{2e}/t-NH_3 [44,45]. If the NH_3 has been produced utilising renewable/clean energy, it is named green NH_3, emitting 0.177 t-CO_{2e}/t-NH_3. Nuclear-sourced NH_3 is named pink in this study, having an emission level at 0.17 t-CO_{2e}/t-NH_3 [44,46].

The emission coefficients used in the analysis were derived from industry reports and peer-reviewed life cycle assessments reflecting current industrial NH_3 production processes. These sources were chosen to ensure realistic assumptions. While some variation may exist compared to site-specific data, the impact on overall results is expected to remain within an acceptable range of uncertainty.

2.3. Proton Exchange Membrane Fuel Cell

The PEMFC stack used in the study was the PowerCellGroup Marine System 200; its technical specifications are shown in Table 2 [36].

Table 2. Specifications of PEMFC.

Parameter	H_2 Fuel Value	Unit
Power	200	KW
Output DC Voltage	580	V
Output Current	400	A
Electrical Efficiency	54% (peak)	-
Fuel Consumption	98.4	Nm^3/h
Fuel Quality	Pure H_2	-

The H_2 consumption of the PEMFC was determined using Equation (2) and performance curves, including the efficiency and SFC curves supplied by the manufacturer [36]. The design of the H_2 tank capacity was intended to provide support for two days, covering potential emergencies and maintenance needs of the decomposition plant. This calculation was predicated on the assumption that the hydrogen is stored in a compressed form at 75 kg/m^3 [47,48].

$$H_2 \text{ Consumption } (t) = SFC \times P_{PEMFC} \times n_{PEMFC} \times t. \quad (2)$$

The operation time in hours is denoted as t, and SFC is interpolated from the curve. P_{PEMFC} and n_{PEMFC} represent the power and number of PEMFCs, respectively. Equation (3) indicates the emissions of PEMFC.

2.4. Battery Cell

A Panasonic NCR18650GA battery cell with a lithium-ion chemistry capacity of 3.45 Ah was utilised in the stack formation. Lithium-ion batteries, known for their higher specific energy and negligible memory effect, were employed in hybrid operation scenarios [48]. The constant-current constant-voltage charging strategy was employed, and the battery set was modelled accordingly. The cell's nominal voltage is 3.6 V, and voltage drop was simulated using SoC-voltage curves from the manufacturer's datasheet [49]. Battery health degradation, represented by state of health (SoH), was obtained from the datasheet.

An energy management strategy (EMS) determined the operational state of batteries and the available SoC. The time-dependent SoC is computed by employing the Coulomb counting method shown in Equation (3) [50].

$$SoC\ (t) = SoC\ (0)\ - \int_0^t \frac{I(t) \times \eta_C}{C_B\ (Ah)}. \quad (3)$$

SoC (0) indicates the initial state of charge at the commencement of the simulation, whereas SoC(t) signifies the revised SoC at t. The EMS keeps the SoC within the range of 20% to 80% during active use to reduce internal resistance, which in turn supports the health and longevity of the battery [50]. The coulombic efficiency (η_C) is taken at 1, with the charging or discharging current denoted as I(t), and the available battery capacity in ampere-hours (Ah) represented by C_B in the equation [51].

The reduction in the battery's capacity was computed throughout its operation, incorporating adjustments influenced by the C-rate. The SoH was determined using Equation (4),

which defines SoH as the ratio of the actual battery capacity (C_a) after degradation to the initial capacity (C_{in}) at the start of operation.

$$\text{SoH (t)} = \frac{C_a\ (\text{Ah})}{C_{in}\ (\text{Ah})}. \quad (4)$$

The SMA Sunny SCS2900 inverter model (SMA, Niestetal, Germany) transforms the DC from the battery to AC for integration into the ship's grid. This inverter operates at an efficiency of 98.4% when converting from 800 V DC to 450 V AC [52].

2.5. Waste Heat Recovery System

An ORC-based WHRS was utilised to generate electricity from the heat of the M/E exhaust waste. The efficiency of the ORC model (η_{ORC}) was adapted at 13.2% from the studies of Konur et al. [53], Konur et al. [54]. The exhaust gas temperature after steam production (T_{in}) in °C and exhaust mass flow rate ($\dot{m}_{ex}$) in kg/s regarding the engine load (%), power (kW), and engine speed (rpm) are indicated in Table 3.

Table 3. The exhaust gas, power, and speed data of the M/E.

Load (%)	Power (kW)	Speed (rpm)	$\dot{m}_{ex}$ (kg/s)	T_{in} (°C)
25	2483	56.9	8.7	190
35	3476	63.7	10	194
50	4965	71.8	13.9	217
71.6	7110	80.9	15.1	205
75	7448	82.1	19.4	208
100	9930	90.4	23.7	235

The simulation's exhaust data, presented in Table 3, was utilised through interpolation based on the acquired real-time M/E data. Equation (5) calculates the generated power by the WHRS ($\dot{W}_{WHRS}$) in kW [55].

$$\dot{W}_{WHRS} = \dot{m}_{ex} \times (T_{in} - T_{out}) \times C_p \times \eta_{ORC}. \quad (5)$$

T_{out} represents the exit temperature from the ORC, set at 100 °C, while C_p denotes the specific heat capacity of the exhaust gas at constant pressure. This value, taken as 1.089 kJ/kgK, reflects the thermal energy exchanged by a unit mass of exhaust gas per unit temperature change [56].

2.6. Marine Diesel Generators

The simulation determined the required engine power and active generators at 1-min intervals. Generator load and power were simulated for hybrid scenarios, with SFC interpolated from D/G datasheets. Based on the approach of Yuksel and Koseoglu [24], load sharing activated additional generators when power exceeded 85% capacity, balancing load by frequency and power factors. Fuel consumption was calculated by multiplying each generator's SFC, required power, and operation time.

2.7. Environmental Model

The emissions from the hybrid configurations and base scenario were computed using the emission coefficients. Table 4 demonstrates the upstream emission coefficients (UEC) and operational emission coefficients (OEC) to calculate operational emissions (OEs) and upstream emissions (UEs).

Table 4. UEC and OEC.

UEC (g UE/g OE)						
Fuel	CO_2	N_2O	CH_4	NO_x	SO_x	Reference
HFO	0.147	0.004	0.879	0.010	0.102	[57,58]
LNG	0.131	0.004	0.879	0.007	* 0.158	[57–59]
H_2	* 110.902	0.000	0.000	* 0.191	* 0.141	[57,58]
OEC (g emission/g fuel)						
Fuel	CO_2	N_2O	CH_4	NO_x	SO_x	Reference
HFO	3.114	0.00015	0.00006	0.903	0.025	[60]

* Unit is g/kWh.

This study adopted a streamlined well-to-wake approach, focusing on the operational and production phase of the fuel pathways and excluding the energy consumption and carbon emissions associated with the manufacturing of FCs and battery systems. While this allows for a consistent and comparable analysis of fuel-related emissions, it introduces limitations, particularly for battery systems, which can involve significant embodied energy and associated emissions during production. The manufacturing phase for FCs and batteries can lead to a deviation of around 20–30% higher emissions compared to the operational phase alone [61]. Upstream and operational emissions were weighted equally, utilising emission coefficients sourced from the literature.

The 100-year global warming potential (GWP100) was demonstrated in the calculation of CO_{2e}, as shown in Equation (6) [62].

$$CO_{2e} = CO_2 + 265 \times N_2O + 28 \times CH_4. \quad (6)$$

The coefficients for CO_{2e} from the 2024 IMO life cycle assessment guidelines [62] were utilised to compute the GWP of nitrous oxide (N_2O) and CH_4. These gases had GWPs approximately 260–273 times for N_2O and 27–30 times for CH_4 greater than CO_2, respectively [58]. The CO_{2e} coefficients for NH_3 production methods are provided in Section 2.2.

2.8. Economic Model

To reduce uncertainty, a scenario-based approach was employed to calculate the LCOE for 2025 and 2040, incorporating projected energy and carbon prices from reliable sources, including currently limited applications, like the Emission Trading System, and academic literature. The primary aim was to illustrate how variations in price levels influence system performance, particularly identifying the carbon price threshold at which renewable energy options become competitive.

Among various methodologies available for techno-economic evaluation, LCOE was selected due to its ability to provide a single, consistent indicator of economic performance across different fuel and technology configurations. It allows for directly comparing energy generation options by accounting for all relevant costs, capital, operational, maintenance, and fuel over the system's lifetime. Moreover, LCOE is one of the most widely used and recognised metrics in energy system analysis, which enhances the comparability and relevance of the findings within the broader academic and industry discourse [63].

The LCOEs was used to gauge each configuration's economic performance. The main instrument of choice for evaluating the unit costs of various baseload technologies at the

plant level throughout their operating lives is LCOE [64]. Equation (7) shows how the LCOE is calculated [65].

$$\text{LCOE}\left(\frac{\text{USD}}{\text{kWh}}\right) = \frac{\sum_{t=1}^{LT} \frac{(C_{plant}+C_{fuel}+C_{o\&m})\ (\text{USD})}{(1+r)^n}}{\sum_{t=1}^{LT} \frac{P_{gen}\ (\text{kW}) \times t(\text{h})}{(1+r)^n}}. \quad (7)$$

The installation cost is C_{plant}, the fuel cost is C_{fuel}, and operation and maintenance costs are represented by $C_{o\&m}$ in Equation (7). The plant's generated total power (P_{gen}) and operation time (t) were calculated from the operational data. Plant lifetime (LT) was assumed to be 20 years, and the discount rate (r) was taken at 10% [64,66]. Table 5 demonstrates the C_{plant} and $C_{O\&M}$ of the equipment.

Table 5. Lifetime, installation, and operational costs of systems.

Equipment	C_{plant}—2025	C_{plant}—2040	Unit	$C_{o\&m}$	LT (Years)	Reference
PEMFC	2540.46	1304.04	USD/kW	1.50%	10 years or 40,000 h	[67,68]
MDE	605,997	605,997	USD	1.50%	20	[69]
HFO Storage	1497	1497	USD/m^3	1%	20	[69]
NH_3 Storage	3,145,236	2,028,677	USD	1%	20	[70]
NH_3 Cracker	2,648,824	1,708,491	USD	6%	20	[71,72]
H_2 Storage	460	243.5	EUR/kg	1%	20	[73]
H_2 P/T	2440	2440	EUR/kW	4%	10	[73]
NH_3 Catalyst/Adsorber	31,083	31,083	USD	N/A	N/A	[72]
ORC WHRS	1,348,579	1,348,579	USD	1.50%	20	[53]
Battery Cell	11.86	11.86	USD	1%	Usage dependent	[74]

The calculation of $C_{o\&m}$ was done by multiplying the percentage by C_{plant}, and the analysis was carried out using the United States dollar (USD). The pound (GBP) and Euro (EUR) to USD exchange rate were set at 1.27 and 1.1, respectively. The rates from the relevant data year and the most recent Chemical Engineering Plant Cost Index (CEPCI) were used to adjust the prices from prior years. According to Maxwell [75], the most recent CEPCI was 798.8 for June 2024 (the most recently announced value). Table 6 indicates the C_{fuel} and carbon price assumptions for 2025 and 2040.

Table 6. Carbon price and C_{fuel} (USD/kg—Fuel) for 2025 and 2040 regarding low/high cases.

Fuel	2025	2040 Low	2040 High	Reference
Grey NH_3	0.229	0.229	0.229	[46]
Blue NH_3	0.372	0.100	0.250	
Green NH_3 by Nuclear	0.918	0.075	0.225	[46,76]
Green NH_3 by Renewable	1.055	0.222	0.480	
Green H_2	3.750	2.334	3.144	[77]
HFO	0.663	0.854	0.971	[78–80]
Carbon Price	0.077	0.155	1.285	

The current C_{fuel} of HFO was obtained from ShipandBunker [79] for global average. Fuel price data used in this study were obtained from reputable literature sources to ensure consistency with established projections and reflect the most credible and widely accepted estimates. Given the inherent uncertainties of future fuel pricing, both low and high projection cases were adopted. These scenarios were defined based on boundary conditions derived from fuel price trends, offering a more comprehensive understanding of potential

economic outcomes. A similar approach was applied to the carbon pricing collected from the literature by fuel price projections.

2.9. Multi-Criteria Decision-Making

The Complex Proportional Assessment (COPRAS) method has effectively ranked the alternatives. This method facilitates a clear and comprehensive comparison by evaluating one alternative's relative merits and drawbacks against others [81,82]. It ensures the optimisation of criteria influenced by multiple factors by considering the utility level and relative importance [83].

The method relies on linear normalisation, standardising diverse criteria by converting them to a uniform scale, thus facilitating direct comparisons. Additionally, it integrates the weighted significance of each criterion, allowing decision-makers to express and incorporate their preferences and priorities into the evaluation framework [84]. This method is frequently utilised in decision-making contexts characterised by uncertainty or ambiguous outcomes [81,85].

The assessment criteria were determined as total CO_{2e}, total other emissions (summation of SO_x and NO_x), and LCOE. Since the LCOE depends on the years and economic projection scenarios, the ranking regarding 2025, 2040 Low, and 2040 High cases were assured. The entropy method introduced by Shannon [86] determined criterion weights, which encompass three stages. The initial step is to normalise the decision matrix using Equation (8) [87].

$$r_{ij} = \frac{f_{ij}}{\sum_{t=1}^{n} f_{ij}}. \quad (8)$$

where f_{ij} depicts the data point to be normalised, n is the number of criteria, and r_{ij} represents the normalised data. The next stage is the calculation of entropy (e_j) employing Equation (9) [87].

$$e_j = \frac{1}{\ln(n)} \times \sum_{i=1}^{m} \ln(r_{ij}),\ j = 1,\ 2,\ \ldots .n. \quad (9)$$

where m represents the total row number. The final stage computes the weights (w_j) utilising Equation (10) [87].

$$w_j = \frac{1 - e_j}{\sum_{i,j=1}^{n} 1 - e_j}. \quad (10)$$

After determining the weights, the normalised matrix was multiplied by the relative w_j, and the weighted normalisation matrix (N_{ij}) was obtained for the COPRAS. Using Equations (11) and (12), the beneficial (B_i) and cost indexes (C_i) were obtained [88].

$$B_i = \sum_{j=1}^{n} N_{ij},\ i = 1, \ldots, k \text{ beneficial criteria}, \quad (11)$$

$$C_i = \sum_{j=k}^{n} N_{ij},\ i = k+1, \ldots, m \text{ cos t criteria}. \quad (12)$$

The relative significance of alternatives (Q_i) was calculated employing Equation (13) [89].

$$Q_i = B_i + \frac{\min(C_i) \times \sum_{i=1}^{n} C_i}{C_i \times \sum_{i=1}^{n} \frac{\min(C_i)}{C_i}}. \quad (13)$$

The final stage of the COPRAS involves the calculation of utility degrees (UD_i) utilising Equation (14) and ranking determination using UD_i values [89].

$$UD_i = \frac{Q_i}{\max(Q_i)} \times 100\%. \quad (14)$$

A higher UD_i means a higher ranking for the configuration [88]. The validity of the COPRAS methodology has been assessed using a sensitivity analysis technique as proposed by Triantaphyllou and Sánchez [90].

Let $\delta'_{k,i,j}$ (for $1 \leq I < j \leq m$ and $1 \leq k \leq n$) represent the minimum adjustment required in the assigned weight W_k of criterion k, to achieve a reversal in the ranking positions of alternative Ai and Aj, as illustrated in Equation (15) [90].

$$\delta'_{k,i,j} < \frac{P_j - P_i}{a_{j,k} - a_{i,k}} \times \frac{100}{w_k}, \text{ if } a_{j,k} > a_{i,k}, \delta'_{k,i,j} > \frac{P_j - P_i}{a_{j,k} - a_{i,k}} \times \frac{100}{w_k}, \text{ if } a_{j,k} < a_{i,k.} \quad (15)$$

Pj and Pi represent the weighted normalised decision matrix elements for the respective rows in this context. The normalised matrix values are defined as $a_{j,k}$ and $a_{i,k}$. The following condition in Equation (16) should be met for the value of $\delta'_{k,i,j}$ [90].

$$\frac{P_j - P_i}{a_{j,k} - a_{i,k}} \leq w_{k.} \quad (16)$$

No weight adjustment can make Aj rank higher when alternative Ai consistently outperforms Aj across all criteria (aik $\geq$ ajk for every k). A criterion is classified as redundant if altering its weight has no impact on the rankings of any alternatives, allowing it to be eliminated from consideration [90].

2.10. Uncertainty Analysis

Uncertainty serves as a metric for the validity of results and is vital for assessing the appropriateness of data in informed decision-making across various domains [91]. Statistical techniques, particularly uncertainty analysis, are instrumental in pinpointing scenarios impacted by uncertainty while improving data accuracy [92]. Varying levels of uncertainty are integrated using Equation (17) [93].

$$U_R = \sqrt{\left[\left(\frac{\delta R}{\delta x_1} U_1\right)^2 + \left(\frac{\delta R}{\delta x_2} U_2\right)^2 + \ldots + \left(\frac{\delta R}{\delta x_n} U_n\right)^2\right]}. \quad (17)$$

In Equation (17), U values denote the partial uncertainties of individual parameters (x_1, x_2,...x_n), U_R demonstrates the uncertainty of the merged calculation, while R is the utilised parameter for each independent metric [94].

An uncertainty analysis of the fuel consumption model was conducted to assess its reliability. Two main sources of uncertainty were identified. Initially MDEs' fuel usage was calculated from the SFC data provided by the manufacturer for proposed systems. In the baseline scenario, the discrepancy between the sensor data and the model outputs was 5.63%. Moreover, the fuel consumption efficiencies exhibited a 2% error margin reflected in the accompanying data sheets. Utilising Equation (17), the overall uncertainty calculated by the model was determined to be 5.98%.

3. Results

The environmental analysis highlights variations in CO_{2e}, NO_x, and SO_x emissions for systems C1 and C2 using grey, blue, pink, and green NH_3 as cracker feedstock. Emissions

from the decomposition system influenced upstream and operational pollutant levels. NH_3 production emissions were excluded, focusing only on those required by maritime regulations for this study.

The C1 and C2 designs required 304 and 298.12 t of H_2 to run PEMFCs for 1.96 years. The current HFO tank capacity (467 m^3) powers the D/Gs for 180 days. To maintain the same bunkering capacity with H_2, the required tank sizes would be 1199.96 m^3 and 1176.76 m^3, respectively. These values can be reduced to 650.10 m^3 and 624.62 m^3 with NH_3 cracking, including 40.11 m^3 and 39.33 m^3 H_2 storage tanks for two days. The NH_3 requirements of the decomposition system to produce the same amount of H_2 on board were set at 1653.43 t for C1 and 1586.47 t for C2. Limiting the capacity to the base value of 467 m^3, the NH_3 tanks would provide fuel for 125.98 and 131.53 days, respectively, including two days of H_2 storage requirements given earlier. The economic analysis was conducted based on the 180-day values. Figure 4 illustrates the hourly power output from the PEMFC plants in both C1 and C2 configurations, along with the corresponding hourly power availability of the WHRS system.

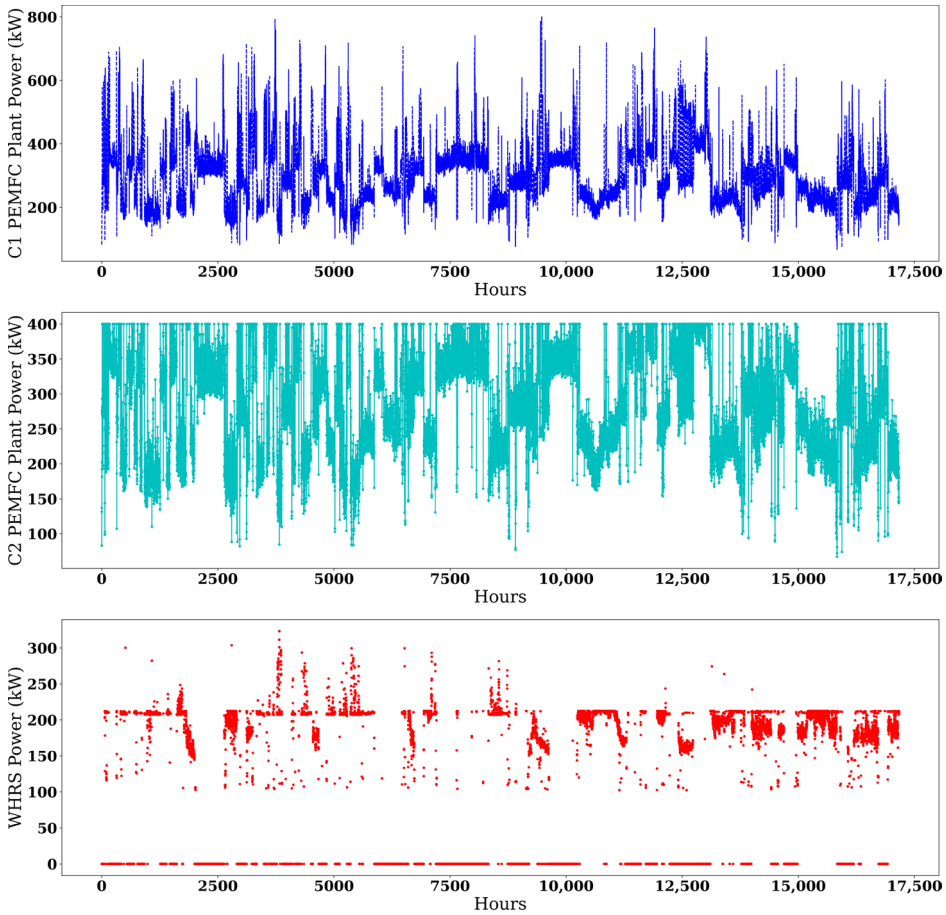

Figure 4. Power outputs from the PEMFC and WHRS in the examined configurations.

The total electrification operation time reached 17,169.6 h. C1 operates without utilising the MDE, resulting in zero HFO usage, and relies mainly on PEMFCs, with minimal battery usage limited to just 5.38 h. During its operation, C1 primarily employed two FCs, which accounted for 75.74% of the total operational time (13,003.72 h). A single PEMFC was used for 14.20% of the time (2438.63 h), while three and four PEMFCs were utilised for 9.11% (1563.70 h) and 0.94% (161.43 h), respectively.

C2 uses MDEs for 1262.88 h, consuming 37.84 tons of HFO, and relies on batteries for 1868.32 h. During its operation, 85.86% of the total runtime (14,741.73 h) was conducted

using two PEMFCs, with the remainder carried out by a single PEMFC. The life spans of PEMFCs were calculated as 9.28 years and 4.91 years for C1 and C2. Since the C1 configuration rarely involves the battery for operations and uses it only for emergency responses, Figure 5 illustrates the changes in SoC and SoH over operational hours.

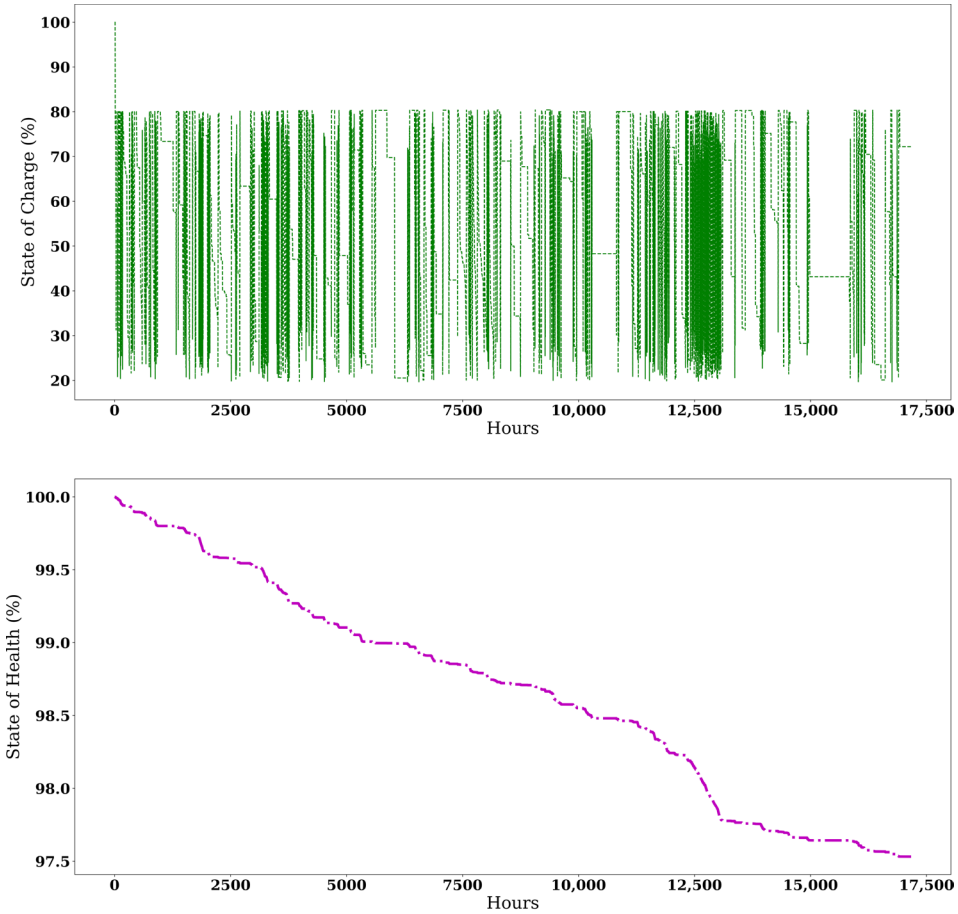

Figure 5. Variation of battery SoC and SoH during the operation of C2.

Based on the usage profile and the final SoH indicated in Figure 5, the estimated battery lifespan for both configurations was calculated over ten years, assuming that 80% SoH marks the end of battery life. In the economic analysis, battery replacements are assumed to occur every ten years. Figure 4 illustrates the CO_{2e} of each configuration regarding NH_3 colour codes for 1.96 years of operation time.

In Figure 6, the emissions represented by the striped bars correspond to operational emissions, while the solid bars indicate upstream emissions. The conventional configuration emitted 5752.82 tonnes of CO_{2e} during operation and 834.56 tonnes upstream, yielding a total of 6587.39 tonnes over 1.96 years. C1 and C2 configurations reduced it by 91.57% and 89.99% by using green H_2-BS. C2 exhibited operational emissions of 119.39 tonnes.

For grey NH_3 decomposition, operational emissions remained unchanged compared to H_2-BS, but upstream emissions significantly increased compared to both the base case and C1/C2 H_2-BS. Upstream CO_{2e} emissions for C1 were 3113.41 tonnes with zero operational CO_2e, while for C2, operational CO_{2e} emissions were 119.39 tonnes, and upstream emissions rose to 3127.59 tonnes. This represents CO_{2e} emissions 5.61 times higher for C1 and 4.74 times higher for C2 than their H_2-BS cases. However, grey NH_3 decomposition with C1 and C2 configurations reduced CO_{2e} by 52.74% and 52.52%, respectively, compared to the MDE configuration.

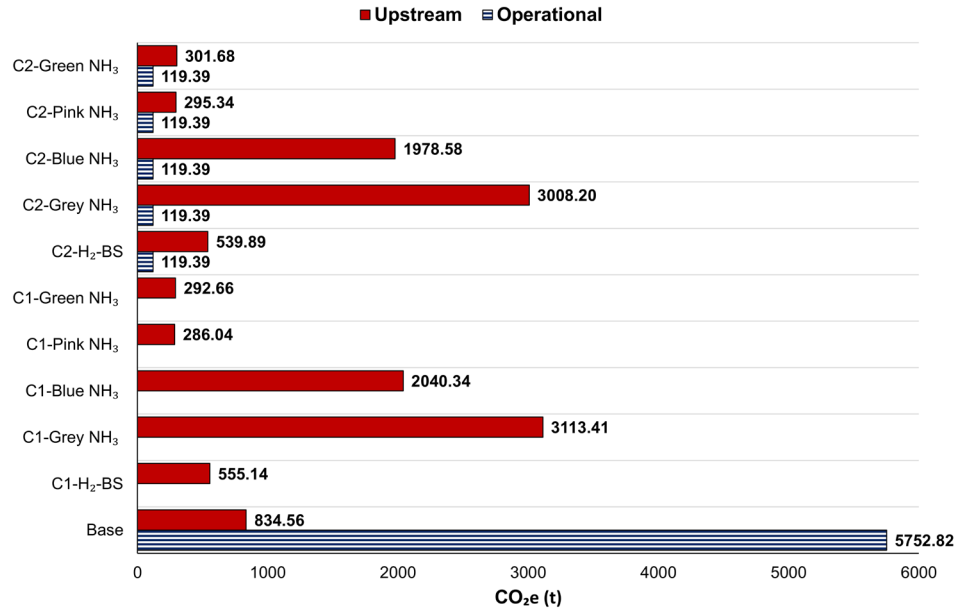

Figure 6. CO_{2e} of configurations regarding the NH_3 production method.

Blue NH_3 cracking reduced upstream CO_{2e} emissions, with C1 and C2 emitting 2040.34 and 1978.58 tonnes, respectively. Compared to the H_2-BS, total CO_{2e} emissions increased 3.68 times for C1 and 3.18 for C2. When benchmarked against the base case, the reduction rates were 69.03% for C1 and 68.15% for C2.

The use of green NH_3 for onboard H_2 production resulted in CO_{2e} emissions of 292.66 tonnes for C1 and 421.07 tonnes for C2. These values represented 47.28% and 36.13% reductions for C1 and C2 configurations, respectively, compared to their green H_2-BS counterparts. Additionally, these emissions corresponded to 95.56% and 93.61% decreases, respectively, compared to the base scenario.

Pink NH_3 decomposition achieved further reductions, with CO_{2e} emissions of 286.04 tonnes for C1 and 414.72 tonnes for C2. These emissions represented 48.47% and 36.13% reductions compared to the H_2-BS configurations and 95.66% and 93.70% compared to the base scenario. Figure 7 demonstrates the SO_x emissions from using different H_2 sources in PEMFCs for 1.96 years.

In the base case, SO_x emissions were at 45.98 tonnes from operational activities, 4.65 tonnes from upstream processes, for a total of 50.23 tonnes, as shown in Figure 7. The C1 and C2 designs, utilising outsourced H_2, emitted 5.73 and 6.52 tonnes of SO_x, representing significant reductions of 88.59% and 87.02%, respectively.

SO_x emissions for grey and blue NH_3 were identical. Using grey or blue NH_3 generally increased SO_x emissions compared to the H_2-BS case. C1 and C2 emitted 6.61 and 7.39 tonnes of SO_x, corresponding to increases of 15.37% and 28.88%, respectively. Despite this, PEMFCs powered by H_2 derived from blue or grey NH_3 under the C1 and C2 designs achieved SO_x reductions of 86.83% and 85.29% compared to the MDE utilisation scenario.

For green NH_3, SO_x emissions were identical regardless of whether nuclear or renewable energy sources were used. SO_x emissions were calculated at 3.31 tonnes for C1 and 4.22 tonnes for C2, equivalent to decreases of 93.42% and 91.61% compared to the base case. Additionally, reductions of 42.31% for C1 and 26.47% for C2 were observed relative to the H_2-BS case. Figure 8 depicts the NO_x emission comparison between NH_3 decomposition system usage and outsourcing H_2.

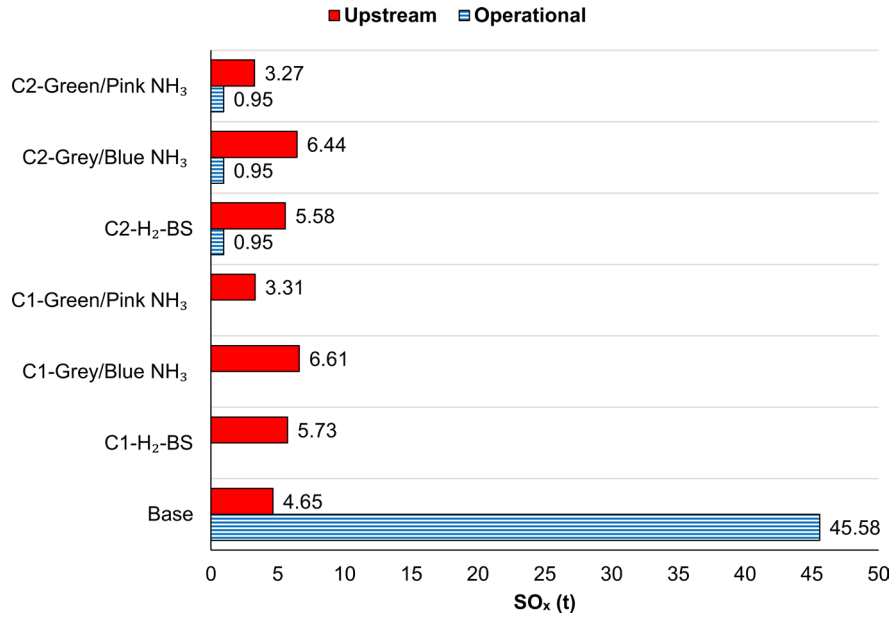

Figure 7. SO_x resulting from configurations regarding the NH_3 production method.

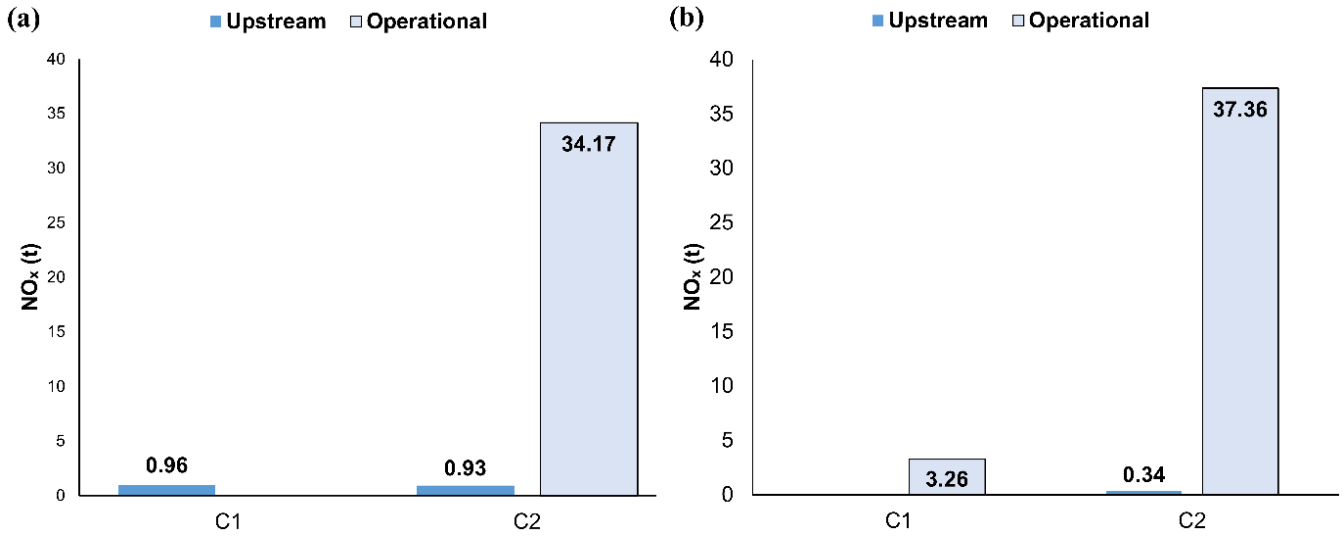

Figure 8. NO_x resulting from (**a**) H_2-BS, (**b**) H_2 derived from NH_3 decomposition onboard.

The upstream and operational NO_x emissions for the base case were calculated at 1646.31 tonnes and 16.46 tonnes, respectively, resulting in a total of 1662.77 tonnes. In the H_2-BS case, C1 emitted only 0.96 tonnes of upstream NO_x emissions, as shown in Figure 8a, corresponding to a 99.94% reduction in total NO_x emissions compared to the base scenario. For C2, total NO_x emissions amounted to 37.70 tonnes, representing a 97.89% reduction. This difference is attributed to the limited consumption of HFO during C2 operations.

The NH_3 cracking system uses heat generated by burning NH_3 for decomposition, leading to a slight increase in operational NO_x emissions. The additional NO_x emissions from this process were calculated at 3.26 tonnes for C1 and 3.19 tonnes for C2. However, since H_2 is no longer outsourced, upstream NO_x emissions were reduced to zero for C1 and 0.34 tonnes for C2, as illustrated in Figure 8b.

For C1, total NO_x emissions increased by 2.3 tonnes compared to the H_2-BS case, but a 99.8% reduction was still achieved relative to the base scenario. A similar trend was observed for C2, where total emissions increased by 7.43% compared to the H_2-BS case, achieving a 97.73% reduction compared to the base configuration. The economic

performance of various NH_3 feedstocks and the H_2-BS case was evaluated by calculating the LCOE as shown in Figure 9 for 2025 and 2040 under low and high projection scenarios.

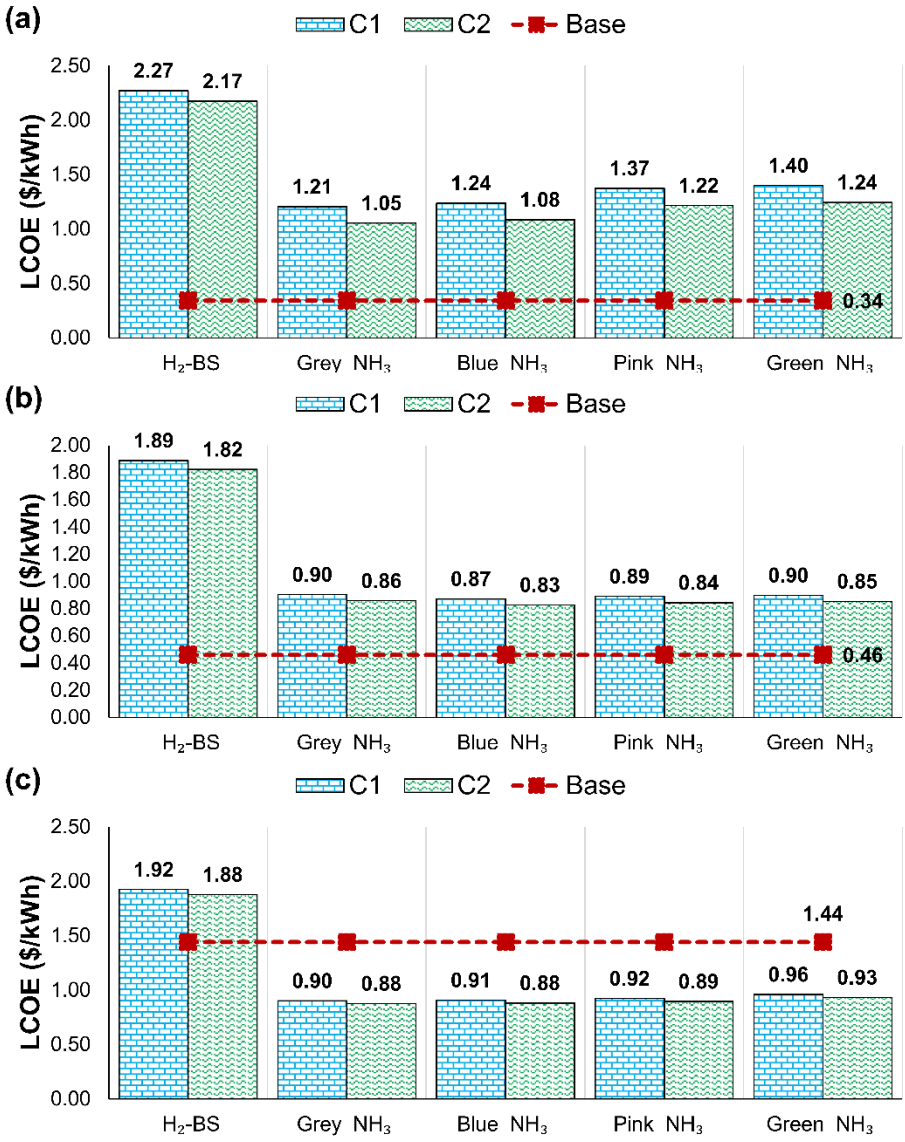

Figure 9. LCOE of different NH_3 feedstocks and H_2-BS for (**a**) 2025, (**b**) 2040-low, and (**c**) 2040-high.

The marine power distribution plant generated 3443.51 MWh of energy annually. The LCOE values presented in Figure 9 were derived by calculating the annual fuel and operation costs and the total investment costs in Appendix C. The base scenario was presented only with H_2-BS, as it remained unchanged in other calculations. Overall, the NH_3 decomposition system was a more economically viable option over the H_2-BS due to the decreased storage costs and lower fuel prices.

In 2025, the base scenario had a LCOE at USD 0.34 per kWh, and the PEMFC scenarios performed worse economically. The most feasible option was C2 with the grey NH_3 cracking system onboard at 1.05 USD/kWh, as shown in Figure 9a. Blue NH_3 with the C2 had a close performance at 1.08 USD/kWh, and considering its environmental superiority over grey NH_3 feedstock, it could be a more attractive option. A similar trend was observed for C1 with a higher level of LCOEs over 1.21 USD/kWh.

Due to the slightly increased carbon prices in the 2040 low-economic scenario, as illustrated in Figure 9b, the LCOEs of NH_3 decomposition scenarios became more viable options. The base-case LCOE rose to 0.46 USD/kWh, whereas the LCOE for H_2-BS de-

creased to USD 1.89 and USD 1.82 per kWh for scenarios C1 and C2, respectively. Among the decomposition pathways, blue NH_3 decomposition offered the lowest LCOE, at 0.83 and 0.87 USD/kWh, followed closely by pink NH_3 cracking.

The high economic projection for 2040, as illustrated in Figure 9c, identified the base case as the worst performer, with an LCOE of USD 1.44 per kWh, which was significantly higher than NH_3-cracking configurations due to the increased carbon prices. The H_2-BS system remained the costliest among all options. Grey and blue NH_3 decomposition under scenario C2 achieved an LCOE of USD 0.88 per kWh, while pink NH_3 reached USD 0.89 per kWh. For scenario C1, the same feedstocks resulted in LCOEs ranging between USD 0.90 and USD 0.92 per kWh. These findings underscore that only implementing higher carbon taxes makes NH_3 decomposition scenarios more cost-competitive than fossil fuel utilisation.

An MCDM analysis using the COPRAS methodology integrated with the entropy weighing method was conducted to combine the environmental and economic studies. The CO_{2e} and other emissions as the environmental indicator and LCOE as the financial performance index were taken in the analysis. Table 7 indicates the criteria weights based on the economic projection scenario and year.

Table 7. Criteria weights regarding the Entropy Method.

Scenario	CO_{2e}	Other Emissions	LCOE
2025	0.386	0.134	0.480
2040 Low	0.386	0.134	0.480
2040 High	0.384	0.134	0.482

The entropy method successfully assigned weights consistent with the criteria. LCOE received the highest weight, ranging from 0.478 to 0.480, followed by CO_{2e}, which varied between 0.384 and 0.386, and other emissions at 0.134. The LCOE accounted for 48% of the total weight, while the environmental metrics collectively represented 52%. The detailed results of the entropy method are demonstrated in Appendix D. Table 8 shows the outcomes of the COPRAS calculation stages.

Table 8. COPRAS outcomes.

Configuration	C_i 2025	C_i 2040 Low	C_i 2040 High	Q_i 2024	Q_i 2040 Low	Q_i 2040 High	UD_i 2025	UD_i 2040 Low	UD_i 2040 High
Base	0.26	0.48	0.30	0.03	0.02	0.03	19.78	7.85	13.07
C1 H_2-BS	0.09	0.08	0.08	0.08	0.10	0.10	59.27	48.59	48.92
C1 Grey NH_3	0.10	0.09	0.15	0.07	0.08	0.06	50.19	39.99	26.40
C1 Blue NH_3	0.08	0.07	0.11	0.09	0.10	0.08	62.58	52.27	36.66
C1 Pink NH_3	0.05	0.04	0.04	0.14	0.20	0.21	99.50	100.00	100.00
C1 Green NH_3	0.05	0.04	0.04	0.14	0.20	0.21	97.58	98.94	96.62
C2 H_2-BS	0.09	0.08	0.08	0.08	0.09	0.10	58.46	44.79	47.35
C2 Grey NH_3	0.10	0.10	0.15	0.07	0.07	0.06	51.36	37.75	26.44
C2 Blue NH_3	0.08	0.08	0.11	0.09	0.10	0.08	63.73	47.96	36.17
C2 Pink NH_3	0.05	0.05	0.04	0.14	0.16	0.19	100	82.80	90.42
C2 Green NH_3	0.05	0.05	0.05	0.14	0.16	0.19	98.12	81.98	87.66

The computation of B_i was excluded, and it was taken as zero since all the criteria were the non-beneficial or cost type in the analysis. For instance, the Q_i was calculated for C1 grey NH_3 by computing the ratio of minimum C_i of the criterion and C_i, which was found at 0.10 in 2025. Then, applying Equations (11) and (12), Q_i and UD_i were calculated

at 0.07 and 50.19 for 2025 in Table 8. Figure 10 illustrates the resulting rankings based on the UD_i values shown in the table.

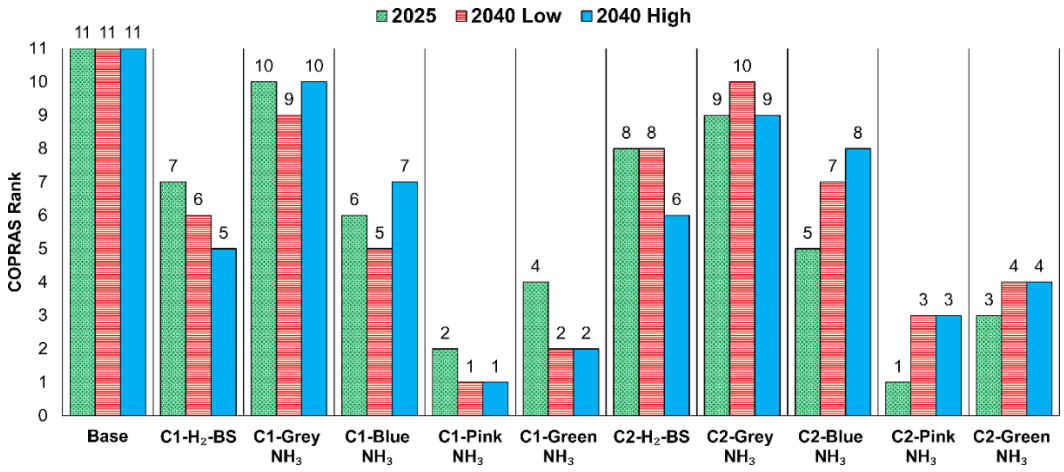

Figure 10. COPRAS ranks of configurations.

The base configuration consistently placed 11th across all economic cases. Similarly, in every economic scenario, the use of grey NH_3 for onboard H_2 production with the C1 and C2 configurations held the 10th and 9th positions, respectively. H_2-BS also performed poorly, with C1 and C2 designs falling between 7th and 8th. Overall, in 2025, the C2 pink NH_3 combination was identified as the most favourable option. However, by 2040, the top position shifted to the C1 pink NH_3 combination. Additionally, by 2040, C1 green NH_3 rose to second place, overtaking C2 pink NH_3, which had previously held that position in 2025.

The sensitivity analysis of COPRAS evaluated 495 instances, classifying them as feasible (F) or non-feasible (NF). Of these, 460 cases were deemed F, while 35 are NF, resulting in a feasibility rate of 92.93%. Among the 460 F instances, 93 were sensitive to changes (with a change rate below 5%), while 367 were resistant to weight changes, demonstrating the validity of the COPRAS method in this analysis. Further details can be found in Appendix E.

4. Discussion

The evaluated hybrid electrification systems reduced ship CO_{2e} emissions to 15.83% with pink NH_3 decomposition. It should be noted that the analysis can involve the FC/battery production phase emissions, elevating CO_{2e} emissions by 20–30%. However, this increase is offset by a substantial overall reduction in emissions compared to conventional systems [61]. The potential for emissions reduction increases to approximately 50% with the implementation of zero-carbon electrification alongside LNG-DF engines in the propulsion unit. Furthermore, employing LNG-fuelled DF engines within diesel-electric propulsion systems can lead to a CO_{2e} emission decrease of up to 20% while adhering to the EEXI and CII requirements [95]. The turbine technologies demonstrate greater carbon reduction potential than DF engines. Incorporating carbon-free fuels like NH_3 or H_2 in their operation is essential for sustainable energy transitions [96]. However, currently available alternative fuels such as LNG or methanol do not meet the 2050 decarbonisation targets. Bridging this gap requires advanced energy systems and a shift to carbon-neutral fuels [69]. FCs for ship electrification present a favourable avenue for enhancing overall ship energy efficiency when combined with DFs or turbines. Additionally, green H_2 can be regarded as a promising alternative fuel for the shipping industry, facilitating significant emissions reductions and promoting long-term sustainability [96].

The H_2-BS scenario has demonstrated inferior performance compared to the NH_3 decomposition process for H_2 generation on board, both economically and environmentally, particularly when utilising pink and green NH_3 as feedstocks. The H_2-BS scenarios for ship electrification are problematic for marine vessels due to shorter bunker intervals, increased volume requirements [33], and the absence of clearly defined safety protocols [97]. Additionally, the existing H_2 fuel production, storage, and distribution capacity is inadequate to support the comprehensive global deployment of marine vehicles utilising H_2 FC-based hybrid topologies [98]. Consequently, an industrial product such as using NH_3 as a H_2 carrier can address supply challenges by offering enhanced flexibility for these systems [15].

NH_3 is rich in H_2 and storable at ambient temperature and pressure and presents an effective medium for H_2 storage, even though it is toxic [99]. Nuclear energy has emerged as a significant source of NH_3 production in the analysis, characterised by low costs, and reduced emissions. Green NH_3, while following closely in emissions performance, is hindered by its higher production costs, resulting in its lower ranking than pink NH_3 options. Nuclear-sourced or pink NH_3 demonstrates significantly lower GHG emissions than the currently available and widely used industrial methods [100]. For instance, according to Bicer and Dincer [101], nuclear-based NH_3 production results in a significantly lower GWP compared to SMR. Specifically, SMR-based grey NH_3 production emits approximately 2.97 kg CO_{2e} per kilogram of NH_3, whereas nuclear-based production emits only about 0.23 kg CO_{2e} per kilogram, indicating a 92% reduction in GWP.

The maritime industry has started to see nuclear energy as a viable alternative, and the possible usage of onboard nuclear power is beginning to be considered [102]. Considering the public concerns regarding nuclear energy [103], challenges related to uranium sourcing and waste management issues [104], investments in green NH_3 are perceived as a more favourable option [105]. Currently, the Haber–Bosch method, commonly employed for NH_3 production, is highly energy-intensive and generates substantial CO_2 emissions. Although grey NH_3 may provide better economic performance, it does not meet emission targets, making such investments counterproductive. A strategic combination of blue, pink, and grey NH_3 will be essential to achieve forthcoming decarbonisation goals effectively. This integrated approach addresses economic viability and aligns with necessary environmental standards [106]. Enhanced carbon capture in blue NH_3 production and greater utilisation of green energy sources could further reduce costs and environmental impacts for both types of NH_3 [107].

The smaller plant (C2) investment is being prioritised in 2025 due to its immediate benefits. However, projections for 2040 indicate that the larger plant (C1) becomes more advantageous, providing greater long-term returns. The high capital costs of PEMFCs, which require multiple replacements during their lifespan, along with the expenses for WHRS and NH_3 cracking and storage, lead to a higher LCOE for electrification plants, making them less competitive than diesel engines in 2025 economic cases. Nonetheless, by 2040, substantially increased carbon taxes are expected to raise the LCOE of conventional engines, resulting in a more favourable LCOE for FC-based configurations compared to diesel engines [108].

Although there is growing interest in NH_3 as a fuel, the current technology is still theoretical and requires practical validation in real-world marine environments. For instance, utilising NH_3 in combustion engines presents significant challenges due to its corrosive properties, which can lead to the deterioration of critical engine components such as pistons, cylinders, and valves [14]. Furthermore, the storage and transportation of NH_3 necessitate stringent safety measures, as any leaks can pose severe health hazards. These factors underscore the need for careful consideration and robust engineering solutions when integrating NH_3 into existing fuel systems [109]. NH_3-powered smaller engines and

NH_3 as an H_2 carrier for FC-based ship electrification represent a more feasible initial stage for implementation [110,111].

5. Conclusions

The study evaluated two distinct PEMFC/battery/WHRS configurations within a marine power distribution system integrated with an NH_3 decomposition system, considering grey, blue, pink, and green NH_3 production methods. The main findings derived from this study can be listed as follows:

Environmental analysis demonstrated that the overall performance of the NH_3 decomposition system with pink and green NH_3 is superior to that of green H_2-BS.

- SO_x emissions mildly increased due to grey and blue NH_3, while green/pink NH_3 cracking performed better than H_2-BS.
- NO_x emissions slightly rose because of the onboard NH_3 decomposition system compared to H_2-BS.
- Economic analysis depicted that the NH_3 decomposition system is more economically viable than H_2-BS due to lower storage costs and fuel prices.
- Increased level of carbon penalties increased the economic viability of a larger PEMFC plant (C1) with pink/green NH_3-decomposition system.
- In the 2040-high cases, NH_3 cracking onboard was more cost-beneficial than the base case.

Limitations of the study are listed as follows:

- In the economic assessment, it has been postulated that the costs of equipment, for which future projections are lacking, will remain stable.
- The environmental analysis included only emissions from the NH_3 cracking system with available emission coefficients.
- The results are based on selected emission and efficiency coefficients sourced from current industrial data and literature; these represent the best available estimates at the time of the study. However, the outcomes may vary as these parameters are subject to change with future technological advancements in NH_3 production and related systems.
- This study uses a well-to-wake approach, excluding manufacturing emissions of FCs and batteries. As a result, the systems' environmental impact may be slightly underestimated due to their production emissions.
- The scrap values of FC and batteries have been excluded from the analysis.

Although based on a bulk carrier, this study's methodology offers insights applicable to other ship types, including container vessels and tankers. It is important to note that operational differences specific to ship types and equipment, such as tank heating or cargo handling, may affect load demand and influence emission reduction potential slightly.

This research adds to the existing literature by delivering an in-depth analysis of NH_3 decomposition systems for the onboard H_2 production utilised in PEMFCs within ship electrification systems. The impact of different NH_3 production methodologies on the environmental and economic performance was investigated in detail. The study's findings can benefit academicians working on maritime decarbonisation or NH_3 cracking areas, ship designers, and powertrain manufacturers willing to enhance systems for marine vessels.

Future research will investigate the integration of PV systems, power take-in/power take-off (PTI/PTO) technologies, and other suitable alternative energy sources alongside FCs and onboard hydrogen production systems. The optimisation of sizing for these systems will be a key focus of this investigation. A more comprehensive evaluation would benefit from incorporating full life cycle assessments that account for the embodied energy

and emissions from the production of battery and FC systems. Incorporating a detailed sensitivity analysis to evaluate the effects of price uncertainties on system performance and investment decisions would constitute a valuable direction for future research, offering deeper insights into the robustness and adaptability of the modelled scenarios.

Another research direction may prioritise a comprehensive risk assessment of the proposed system design, focusing on the bunkering, storage, and transfer of H_2 and NH_3 onboard. Identifying potential hazards and mitigating associated risks is vital for ensuring safety and regulatory compliance. Given that the analysis primarily considers theoretical aspects in an "ideal environment", it is crucial to acknowledge that real marine conditions present challenges such as vibrations, impacts, and possible chemical interactions with NH_3.

Additionally, exploring various cracking systems and conducting thermodynamic analyses of NH_3 decomposition processes can enhance overall system efficiency. This application may aim to identify optimal methods for onboard H_2 production, facilitating integration into the broader energy system and promoting sustainability in NH_3 utilisation as a marine fuel. Furthermore, implementing FCs in conjunction with decomposition systems across different vessel types presents an opportunity for innovation. Assessing the integration of FCs with diverse vessel designs will provide insights into performance metrics, operational feasibility, and economic viability in various maritime contexts. Enhancing these areas is essential for the safe and efficient adoption of H_2 and NH_3 as alternative marine fuels, ultimately contributing to the decarbonisation of the shipping industry.

Author Contributions: Conceptualisation, O.Y., E.B.-D. and M.A.; methodology, O.Y., E.B.-D., J.W. and G.V.S.; software, O.Y.; validation, O.Y. and N.T.; formal analysis, O.Y., E.B.-D., M.A., G.V.S., M.C.D.P. and M.P.; investigation, O.Y., E.B.-D., A.S., D.H. and G.V.S.; resources, E.B.-D., J.W., N.T., M.C.D.P. and M.P.; data curation, N.T., O.Y., M.C.D.P. and M.P.; writing—original draft preparation, O.Y., E.B.-D., A.S., D.H., G.V.S. and J.W.; review and editing, O.Y., E.B.-D., A.S., D.H., G.V.S., M.C.D.P., M.P. and J.W.; visualisation, O.Y., E.B.-D., A.S., D.H., G.V.S., M.C.D.P. and J.W.; supervision, J.W., E.B.-D., M.C.D.P. and M.P.; project administration, E.B.-D., A.S. and M.P.; funding acquisition, E.B.-D., A.S., M.A., N.T. and M.P. All authors have read and agreed to the published version of the manuscript.

Funding: This research was funded by Retrofit Solutions to Achieve 55% GHG Reduction by 2030, grant number 10064483 from UKRI and from EU (grant number: Horizon Europe 101096068).

Institutional Review Board Statement: Not applicable.

Informed Consent Statement: Not applicable.

Data Availability Statement: The dataset generated during this study is available in Zenodo and can be accessed via the persistent identifier https://doi.org/10.5281/zenodo.15457758. This dataset is made available under the license: Creative Commons Attribution 4.0 International License (CC-BY 4.0). For additional inquiries regarding the dataset, please contact the corresponding author.

Conflicts of Interest: Author Nikolaos Tsoulakos was employed by the company Laskaridis Shipping Co., Ltd. Milad Armin was the owner of the company Enki Marine Technology Consultancy. The remaining authors declare that the research was conducted in the absence of any commercial or financial relationships that could be construed as a potential conflict of interest.

Nomenclature

Abbreviation or Symbol	Explanation	Unit
Ai, Aj	Assessed alternatives in the sensitivity analysis	-
$a_{j,k}$, $a_{i,k}$	Normalised performance values of alternatives A_i and A_j for criterion k in the sensitivity analysis	-
AC	Alternating current	-
B_i	Cost index of beneficial criteria in COPRAS	-

C_a	Actual battery capacity	Ah
C_B	Available battery capacity	Ah
C_i	Cost index of non-beneficial criteria in COPRAS	-
C_{in}	Initial maximum capacity	Ah
C_{fuel}	Fuel prices	USD
$C_{o\&m}$	Operation and maintenance cost	USD
C_p	Specific heat rate of the exhaust	kJ/kg·K
C_{plant}	Capital cost of systems	USD
CEPCI	Chemical Engineering Plant Cost Index	-
CH_4	Methane	-
CO_2	Carbon dioxide	-
CO_{2e}	Equivalent carbon dioxide	-
COPRAS	Complex Proportional Assessment	-
D/G	Diesel generator	-
DC	Direct current	-
e_j	Entropy	-
F	Feasible (in sensitivity analysis)	-
f_{ij}	The data point to be normalised in the entropy method	-
FC	Fuel cell	-
GHG	Greenhouse gas	-
GWP	Global warming potential for 100 years	-
H_2	Hydrogen	-
H_2-BS	Green hydrogen bunkering scenario	-
HFO	Heavy fuel oil	-
I	Current	A
IMO	International Maritime Organization	-
LCOE	Levelised cost of energy	-
LNG	Liquefied natural gas	-
LT	Plant lifetime	Years or hours
m	The number of rows in the entropy method	-
$\dot{m}_{ex}$	Exhaust mass flow rate	kg/s
M/E	Main engine	-
M/V	Motor vessel	-
MCDM	Multi-criteria decision-making	-
MDE	Marine diesel engines	-
N_2O	Nitrous oxide	-
n	Number of criteria in the entropy method	-
N_{ij}	Weighted normalisation matrix in COPRAS	-
n_{PEMFC}	Number of working PEMFCs	-
NF	Non-feasible (in sensitivity analysis)	
NH_3	Ammonia	-
NO_x	Nitrogen oxides	-
OE	Operational (tank-to-wake) emissions	g or t
OEC	Operational emission coefficient	g emission/g fuel)
ORC	Organic Rankine cycle	-
P_i. P_j	Aggregate scores for assessed alternatives in the sensitivity analysis in the weighted normalised decision matrix.	-
P_{gen}	The plant's generated total power	kW
P_{PEMFC}	Power output of one PEMFC	kW

PEMFC	Proton exchange membrane fuel cell	-
PV	Photovoltaic	-
r	Discount rate	-
R	The utilised parameter for each independent metric in the uncertainty analysis	-
r_{ij}	Normalised data in the entropy method	-
SFC	Specific fuel consumption	
SMR	Steam methane reforming	-
SO_x	Sulphur oxides	-
SoC	Stage of charge	-
SOFC	Solid oxide fuel cell	-
SoH	State of health	-
Q_i	The relative significance of alternatives in COPRAS	-
t	Operation time	h
$T_{in,\ ex}$	The inlet temperature of the exhaust (after the exhaust boiler)	K
$T_{out,\ ex}$	Outlet temperature from ORC	K
U	Uncertainty	-
UD_i	Utility degrees in COPRAS	
UE	Upstream (well-to-tank) emissions	g or t
UEC	Upstream emission coefficient	g UE/g OE or g/kWh
w_j	Criteria weights calculated in the entropy method	-
W_k	Criteria weights assessed in the sensitivity analysis	-
WHRS	Waste heat recovery system	
Greek Symbols		
$\delta'_{k,i,j}$	Minimum required adjustment in weight of criterion k to reverse the ranking between alternatives in the sensitivity analysis	-
ΔH_0	Enthalpy change	kJ/mol
η_C	Columbic efficiency	-
η_{FC}	Efficiency of fuel cell	-
η_{ORC}	Organic Rankine cycle efficiency	-

Appendix A

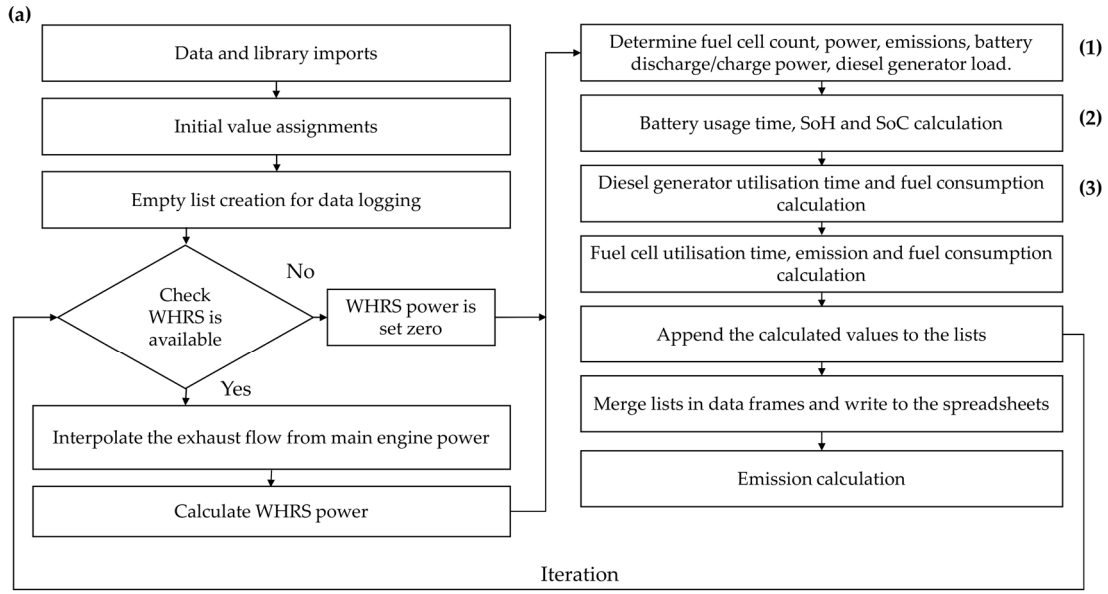

Figure A1. *Cont.*

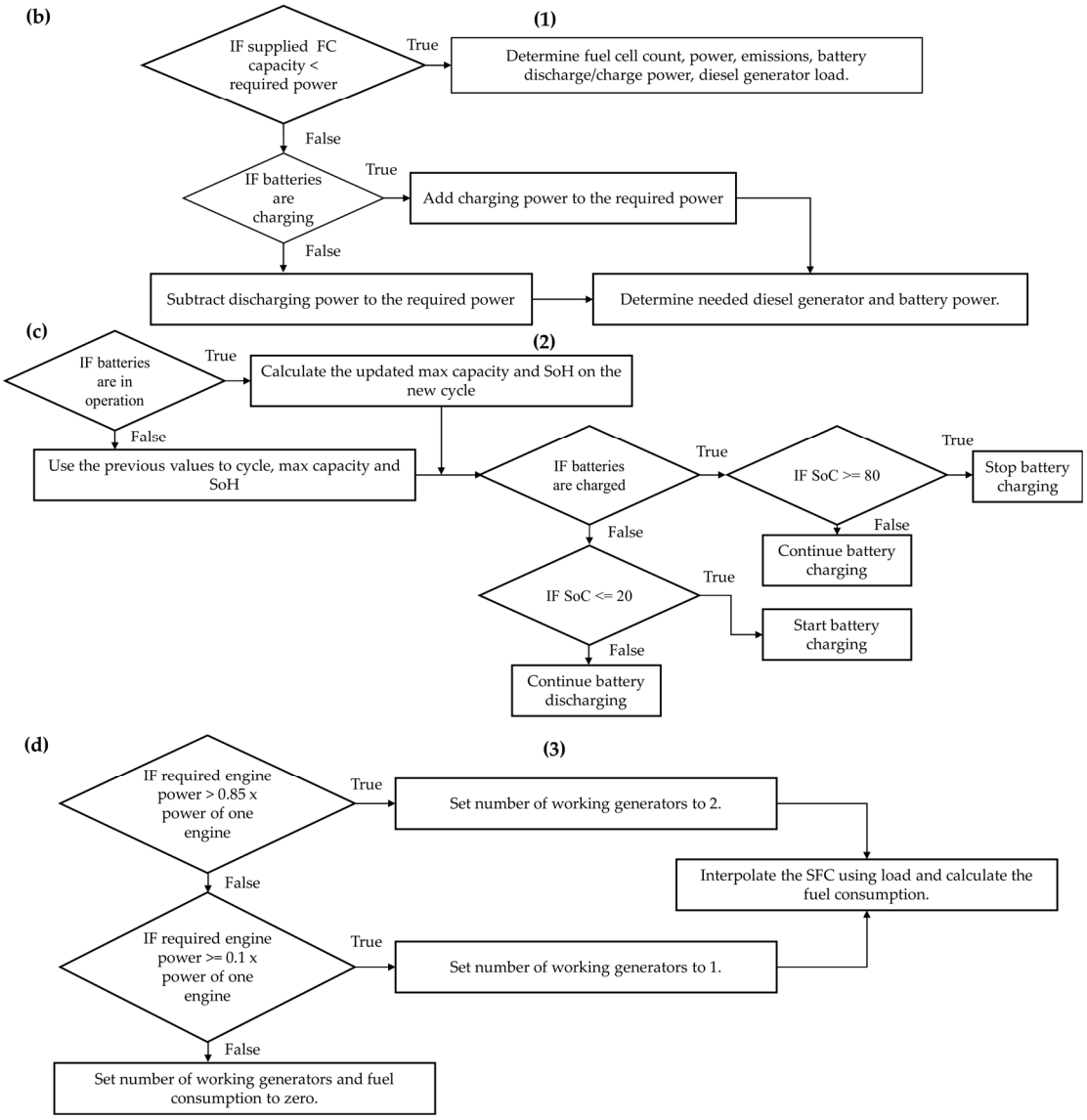

Figure A1. Simplified algorithm scheme: (**a**) general process, (**b**) FC determination details, (**c**) battery operation, and (**d**) D/G fuel consumption calculation.

Appendix B

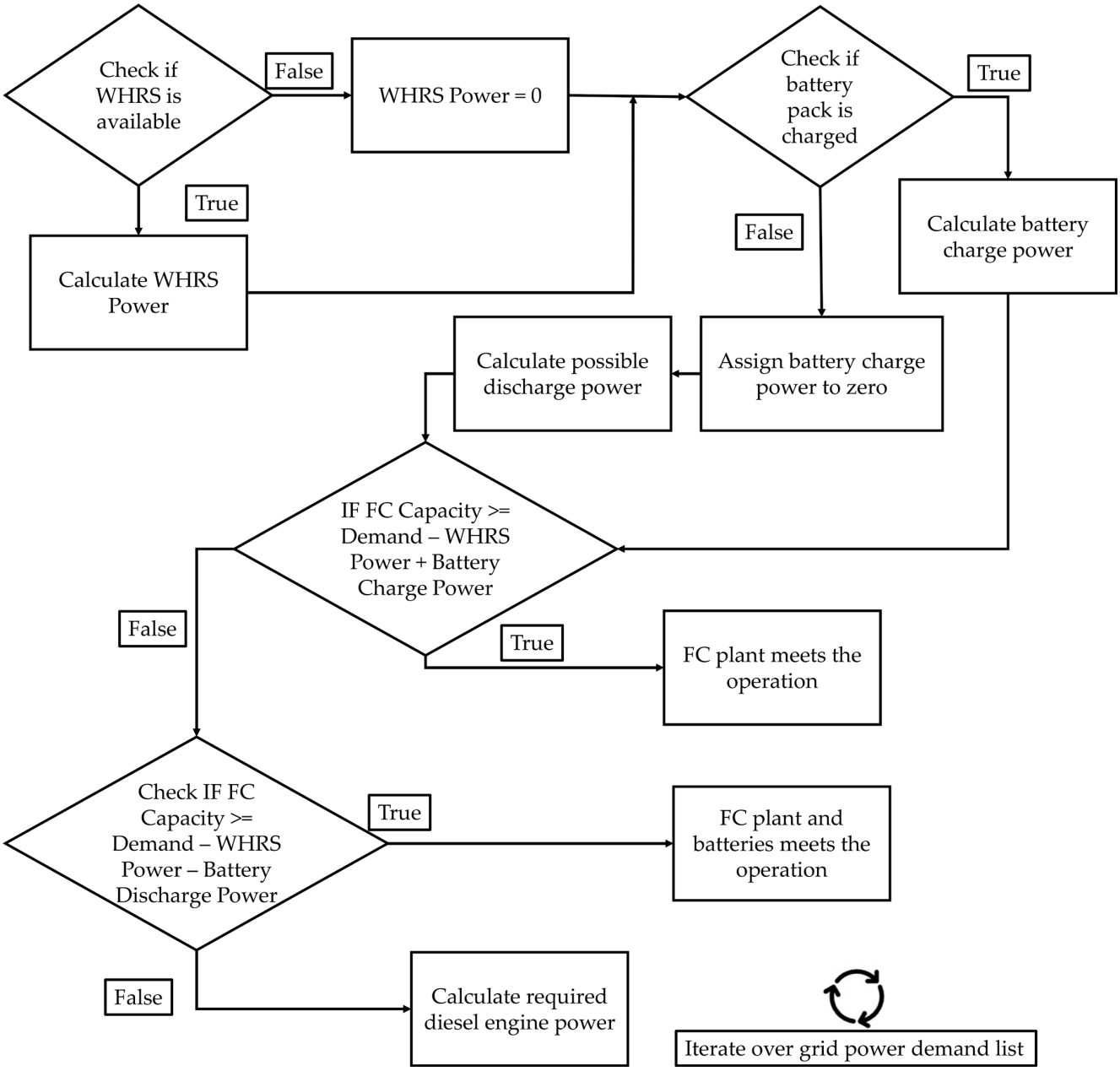

Figure A2. Simplified energy management strategy for establishing the hierarchy among power equipment.

Appendix C

Table A1. Installation, operation, and fuel costs of the configurations.

C_{plant}	FC		Battery		NH_3 Storage P/T		H_2 Storage P/T		HFO Storage	NH_3 Cracker		WHRS		MDE		Total
	2025	2040	2025	2040	2025	2040	2025	2040	2025/2040	2025	2040	2025/2040		2025/2040	2025	2040
C1	6,097,104	3,129,703	685,840	442,367	9,435,707	6,086,031	8,860,660	8,283,109	0	0	2,648,824	1,708,491		1,348,579	1,348,579	622,987
C2	5,080,920	2,608,086	234,401	151,189	9,053,576	5,839,556	6,625,170	8,205,986	14,530	14,530	2,541,550	1,639,300		1,348,579	1,348,579	1,245,974
Base	N/A	N/A	N/A	N/A	N/A	N/A	N/A	N/A	700,157	N/A	N/A	N/A		1,868,962	2,569,119	2,569,119
$C_{O\&M}$	FC		Battery		NH_3 Storage P/T		H_2 Storage P/T		HFO Storage	NH_3 Cracker		WHRS		MDE	Total	
	2024	2040	2024	2040	2024	2040	2024	2040	2024/2040	2024	2040	2024/2040		2024/2040	2024	2040
C1	91,457	46,946	6858	4424	94,357	60,860	217,439	211,663	0	0	31,083	20,049		20,229	20,229	9345
C2	76,214	39,121	2344	1512	90,536	58,396	130,668	125,004	145	145	31,083	20,049		20,229	20,229	18,690
Base	N/A	N/A	N/A	N/A	N/A	N/A	N/A	N/A	7002	N/A	N/A	N/A	N/A	28,034	35,036	35,036
C_{fuel}	H_2—BS				Grey NH_3				Blue NH_3			Pink NH_3			Green NH_3	
	2024		2040	2024	2040	2024	2040	2024	2040	2024	2040	2024	2040	2024	2040—Low	2040—High
C1	581,633		362,008	487,641	193,182	193,182	193,182	313,815	84,359	210,897	774,414	63,269	189,807	889,985	187,277	404,922
C2	587,792		380,817	574,189	189,971	194,686	262,603	305,719	90,270	279,601	747,664	70,034	259,365	858,555	189,020	465,769
Base	N/A		N/A	N/A	N/A	N/A	N/A	N/A	N/A	N/A	N/A	N/A	N/A	838,992	1,243,776	4,624,963

Appendix D

Table A2. Normalised matrix and entropy results.

N_{ij}	CO_{2e}	Other Emissions	LCOE 2025	LCOE 2040 Low	LCOE 2040 High
Base	0.336	0.870	0.023	0.041	0.115
C1 H_2-BS	0.028	0.003	0.156	0.170	0.154
C1 Grey NH_3	0.159	0.005	0.083	0.081	0.072
C1 Blue NH_3	0.104	0.005	0.085	0.078	0.072
C1 Green NH_3 -N	0.015	0.003	0.094	0.080	0.074
C1 Green NH_3-R	0.015	0.003	0.096	0.081	0.077
C2 H_2-BS	0.034	0.021	0.149	0.164	0.150
C2 Grey NH_3	0.160	0.023	0.072	0.077	0.070
C2 Blue NH_3	0.107	0.023	0.074	0.074	0.070
C2 Green NH_3-N	0.021	0.021	0.083	0.076	0.071
C2 Green NH_3-R	0.021	0.021	0.085	0.077	0.074

Table A2. *Cont.*

e_j	CO_{2e}	Other Emissions	LCOE 2025	LCOE 2040 Low	LCOE 2040 High
Base	−0.37	−0.12	−0.09	−0.13	−0.25
C1 H_2-BS	−0.10	−0.02	−0.29	−0.30	−0.29
C1 Grey NH_3	−0.29	−0.03	−0.21	−0.20	−0.19
C1 Blue NH_3	−0.24	−0.03	−0.21	−0.20	−0.19
C1 Green NH_3 -N	−0.06	−0.02	−0.22	−0.20	−0.19
C1 Green NH_3-R	0.00	−0.02	−0.22	−0.20	−0.20
C2 H_2-BS	−0.11	−0.08	−0.28	−0.30	−0.28
C2 Grey NH_3	−0.29	−0.09	−0.19	−0.20	−0.19
C2 Blue NH_3	−0.24	−0.09	−0.19	−0.19	−0.19
C2 Green NH_3-N	−0.08	−0.08	−0.21	−0.20	−0.19
C2 Green NH_3-R	−0.08	−0.08	−0.21	−0.20	−0.19

Appendix E

Table A3. Sensitivity analysis results.

Comparison	CO_{2e}	SO_x + NO_x	LCOE—2025	CO_{2e}	SO_x + NO_x	LCOE-2040 L	CO_{2e}	SO_x + NO_x	LCOE 2040 H
A1-A2	−0.02	0.00	−0.10	−0.10	0.00	0.00	−1.19	−3.25	2.27
A1-A3	−0.27	0.00	0.09	−0.08	−0.23	0.20	−0.01	0.00	−0.09
A1-A4	−0.08	0.20	−0.11	−0.08	−0.20	0.16	−0.18	−0.46	0.24
A1-A5	0.04	0.12	−0.20	−0.19	0.00	0.01	−0.04	−0.04	−0.13
A1-A6	0.04	0.11	−0.19	−0.19	−0.04	0.04	−0.03	0.00	−0.16
A1-A7	−0.25	0.00	0.03	−0.03	0.00	−0.18	−0.15	−0.03	0.02
A1-A8	−0.20	0.04	−0.05	−0.04	−0.04	−0.14	−0.14	0.00	0.00
A1-A9	−0.30	0.00	0.03	−0.25	0.00	0.00	−0.20	−0.03	0.02
A1-A10	−0.26	0.03	−0.03	−0.25	−0.03	0.02	−0.20	0.00	0.00
A1-A11	−0.40	−1.07	0.08	−0.35	−0.95	0.05	−0.37	−1.01	−0.04
A2-A3	−0.45	0.01	0.24	−0.08	−0.24	0.21	0.30	0.85	−0.70
A2-A4	−0.10	0.26	−0.12	−0.08	−0.21	0.17	−0.01	0.00	−0.09
A2-A5	0.05	0.13	−0.21	−0.20	0.00	0.01	−0.03	0.00	−0.16
A2-A6	0.04	0.12	−0.20	−0.19	−0.04	0.04	−0.01	0.04	−0.19
A2-A7	−0.26	0.00	0.04	−0.03	0.00	−0.18	−0.14	0.00	0.00
A2-A8	−0.21	0.04	−0.04	−0.04	−0.04	−0.14	−0.13	0.03	−0.02
A2-A9	−0.31	0.00	0.03	−0.25	0.00	0.00	−0.19	0.00	0.00
A2-A10	−0.27	0.03	−0.03	−0.25	−0.03	0.02	−0.19	0.02	−0.01
A2-A11	−0.41	−1.10	0.08	−0.35	−0.95	0.05	−0.37	−0.99	−0.05

Table A3. *Cont.*

Comparison	CO_{2e}	$SO_x + NO_x$	LCOE—2025	CO_{2e}	$SO_x + NO_x$	LCOE-2040 L	CO_{2e}	$SO_x + NO_x$	LCOE 2040 H
A3-A4	0.12	0.41	−0.34	−0.03	0.00	−0.10	−0.51	−1.41	0.91
A3-A5	0.18	0.16	−0.32	−0.22	0.04	−0.04	−0.04	−0.04	−0.14
A3-A6	0.15	0.15	−0.30	−0.22	0.00	0.00	−0.03	0.00	−0.16
A3-A7	−0.25	−0.01	0.02	−0.02	0.04	−0.25	−0.16	−0.03	0.03
A3-A8	−0.19	0.04	−0.06	−0.03	0.00	−0.20	−0.15	0.00	0.01
A3-A9	−0.30	0.00	0.02	−0.27	0.03	−0.03	−0.21	−0.03	0.02
A3-A10	−0.26	0.03	−0.05	−0.27	0.00	0.00	−0.21	0.00	0.01
A3-A11	−0.41	−1.14	0.08	−0.38	−1.01	0.04	−0.38	−1.04	−0.04
A4-A5	0.21	0.00	−0.31	−0.22	0.04	−0.03	−0.03	0.00	−0.17
A4-A6	0.17	0.00	−0.28	−0.22	0.00	0.01	−0.02	0.04	−0.19
A4-A7	−0.31	−0.08	0.08	−0.02	0.04	−0.25	−0.15	0.00	0.01
A4-A8	−0.23	0.00	−0.03	−0.03	0.00	−0.20	−0.14	0.03	−0.01
A4-A9	−0.35	−0.05	0.06	−0.28	0.03	−0.03	−0.20	0.00	0.01
A4-A10	−0.30	0.00	−0.02	−0.28	0.00	0.00	−0.20	0.02	−0.01
A4-A11	−0.44	−1.24	0.10	−0.38	−1.03	0.04	−0.38	−1.03	−0.05
A5-A6	−0.02	0.00	−0.14	−0.17	−1.05	0.85	0.90	3.00	−2.22
A5-A7	−0.49	−0.10	0.22	2.30	0.05	−2.73	−0.59	−0.01	0.62
A5-A8	−0.34	−0.01	0.04	1.45	−0.33	−1.51	−0.53	0.12	0.50
A5-A9	−0.46	−0.06	0.14	−0.44	0.00	−0.02	−0.55	−0.01	0.34
A5-A10	−0.39	0.00	0.04	−0.43	−0.14	0.09	−0.53	0.07	0.28
A5-A11	−0.51	−1.36	0.15	−0.51	−1.90	0.10	−0.81	−2.27	0.08
A6-A7	−0.53	−0.11	0.25	4.96	1.23	−6.58	−0.66	−0.16	0.77
A6-A8	−0.35	−0.01	0.05	2.32	0.06	−2.78	−0.60	−0.01	0.63
A6-A9	−0.49	−0.07	0.15	−0.48	0.17	−0.16	−0.58	−0.09	0.41
A6-A10	−0.41	0.00	0.04	−0.46	0.00	−0.02	−0.56	−0.01	0.35
A6-A11	−0.52	−1.39	0.15	−0.52	−1.93	0.07	−0.83	−2.35	0.12
A7-A8	0.04	0.23	−0.39	−0.34	−1.13	1.05	0.39	2.36	−1.51
A7-A9	−0.43	0.00	0.02	−1.43	−0.02	0.96	−0.50	0.00	0.00
A7-A10	−0.29	0.10	−0.15	−1.35	−0.20	1.04	−0.46	0.16	−0.10
A7-A11	−0.51	−1.89	0.12	−0.73	−2.05	0.32	−0.92	−3.40	−0.19
A8-A9	−1.22	−0.39	0.71	−1.66	0.21	0.94	−0.57	−0.18	0.12
A8-A10	−0.54	0.00	0.02	−1.54	−0.02	1.04	−0.52	0.00	0.00
A8-A11	−0.63	−2.34	0.22	−0.74	−2.08	0.29	−0.96	−3.58	−0.15
A9-A10	0.01	0.32	−0.54	−0.11	−2.75	2.25	0.10	2.50	−1.60
A9-A11	−0.54	−2.61	0.15	−0.53	−2.60	0.14	−1.23	−5.89	−0.33
A10-A11	−0.66	−3.23	0.30	−0.54	−2.60	0.10	−1.30	−6.33	−0.26

Table A3. *Cont.*

Comparison	CO_{2e}	$SO_x + NO_x$	LCOE -2025	CO_{2e}	$SO_x + NO_x$	LCOE-2040 L	CO_{2e}	$SO_x + NO_x$	LCOE 2040 H
A1-A2	F	F	F	F	F	F	F	F	NF
A1-A3	F	F	F	F	F	F	F	F	F
A1-A4	F	NF	F	F	F	F	F	F	F
A1-A5	F	F	F	F	F	F	F	F	F
A1-A6	F	F	F	F	F	F	F	F	F
A1-A7	F	F	F	F	F	F	F	F	F
A1-A8	F	F	F	F	F	F	F	F	F
A1-A9	F	F	F	F	F	F	F	F	F
A1-A10	F	F	F	F	F	F	F	F	F
A1-A11	F	F	F	F	F	F	F	F	F
A2-A3	F	F	F	F	F	F	F	NF	F
A2-A4	F	NF	F	F	F	F	F	F	F
A2-A5	F	F	F	F	F	F	F	F	F
A2-A6	F	F	F	F	F	F	F	F	F
A2-A7	F	F	F	F	F	F	F	F	F
A2-A8	F	F	F	F	F	F	F	F	F
A2-A9	F	F	F	F	F	F	F	F	F
A2-A10	F	F	F	F	F	F	F	F	F
A2-A11	F	F	F	F	F	F	F	F	F
A3-A4	F	NF	F	F	F	F	F	F	NF
A3-A5	F	NF	F	F	F	F	F	F	F
A3-A6	F	NF	F	F	F	F	F	F	F
A3-A7	F	F	F	F	F	F	F	F	F
A3-A8	F	F	F	F	F	F	F	F	F
A3-A9	F	F	F	F	F	F	F	F	F
A3-A10	F	F	F	F	F	F	F	F	F
A3-A11	F	F	F	F	F	F	F	F	F
A4-A5	F	F	F	F	F	F	F	F	F
A4-A6	F	F	F	F	F	F	F	F	F
A4-A7	F	F	F	F	F	F	F	F	F
A4-A8	F	F	F	F	F	F	F	F	F
A4-A9	F	F	F	F	F	F	F	F	F
A4-A10	F	F	F	F	F	F	F	F	F
A4-A11	F	F	F	F	F	F	F	F	F
A5-A6	F	F	F	F	F	NF	NF	NF	F
A5-A7	F	F	F	NF	F	F	F	F	NF
A5-A8	F	F	F	NF	F	F	F	F	NF
A5-A9	F	F	F	F	F	F	F	F	F
A5-A10	F	F	F	F	F	F	F	F	F

Table A3. *Cont.*

Comparison	CO_{2e}	$SO_x + NO_x$	LCOE -2025	CO_{2e}	$SO_x + NO_x$	LCOE-2040 L	CO_{2e}	$SO_x + NO_x$	LCOE 2040 H
A5-A11	F	F	F	F	F	F	F	F	F
A6-A7	F	F	F	NF	NF	F	F	F	NF
A6-A8	F	F	F	NF	F	F	F	F	NF
A6-A9	F	F	F	F	NF	F	F	F	F
A6-A10	F	F	F	F	F	F	F	F	F
A6-A11	F	F	F	F	F	F	F	F	F
A7-A8	F	NF	F	F	F	NF	NF	NF	F
A7-A9	F	F	F	F	F	NF	F	F	F
A7-A10	F	F	F	F	F	NF	F	NF	F
A7-A11	F	F	F	F	F	F	F	F	F
A8-A9	F	F	NF	F	NF	NF	F	F	F
A8-A10	F	F	F	F	F	NF	F	F	F
A8-A11	F	F	F	F	F	F	F	F	F
A9-A10	F	NF	F	F	F	NF	F	NF	F
A9-A11	F	F	F	F	F	F	F	F	F
A10-A11	F	F	F	F	F	F	F	F	F
Comparison	**CO_{2e}**	**$SO_x + NO_x$**	**LCOE -2025**	**CO_{2e}**	**$SO_x + NO_x$**	**LCOE-2040 L**	**CO_{2e}**	**$SO_x + NO_x$**	**LCOE 2040 -H**
A1-A2	−4.16	0.00	−21.04	−26.52	0.00	−0.48	−309.56	−2433.07	N/F
A1-A3	−68.91	2.43	19.45	−21.95	−172.92	42.36	−3.31	0.00	−18.02
A1-A4	−20.57	N/F	−23.81	−19.88	−149.30	33.79	−45.67	−342.08	49.74
A1-A5	10.97	86.42	−41.15	−50.43	−2.73	1.07	−10.18	−27.36	−27.94
A1-A6	9.51	78.97	−40.13	−50.22	−30.63	7.38	−7.25	−0.10	−33.16
A1-A7	−64.74	−3.50	6.22	−7.22	−0.10	−37.03	−39.31	−23.91	4.54
A1-A8	−50.98	28.82	−9.82	−9.70	−26.13	−29.14	−37.60	−2.03	0.61
A1-A9	−76.77	−2.58	5.63	−64.02	−2.15	−0.15	−52.60	−20.40	3.99
A1-A10	−68.19	23.22	−6.96	−63.63	−24.74	5.01	−51.82	−1.73	0.64
A1-A11	−103.13	−800.74	16.36	−90.91	−706.10	10.42	−97.16	−752.76	−8.21
A2-A3	−117.76	4.27	49.99	−21.74	−180.60	44.26	77.16	N/F	−147.46
A2-A4	−25.29	N/F	−24.60	−19.63	−154.99	35.09	−2.50	0.00	−19.77
A2-A5	13.23	99.34	−44.16	−50.61	−2.75	1.08	−6.75	0.24	−33.70
A2-A6	11.35	89.63	−42.70	−50.39	−30.84	7.43	−3.83	27.47	−38.91
A2-A7	−68.51	−3.72	7.92	−7.09	−0.10	−37.28	−36.85	−1.99	0.26
A2-A8	−53.33	30.27	−9.26	−9.59	−26.30	−29.32	−35.15	19.82	−3.65
A2-A9	−80.04	−2.69	6.84	−64.23	−2.16	−0.15	−50.61	−1.69	0.34
A2-A10	−70.76	24.15	−6.39	−63.84	−24.88	5.05	−49.84	16.93	−3.00
A2-A11	−105.72	−821.69	17.34	−91.15	−708.65	10.46	−95.79	−741.92	−11.32
A3-A4	31.76	N/F	−70.62	−6.84	0.00	−20.39	−133.92	−1054.73	N/F
A3-A5	45.61	N/F	−67.43	−56.21	31.78	−7.30	−10.58	−28.93	−28.51
A3-A6	39.47	N/F	−62.89	−55.71	−3.01	0.59	−7.48	−0.10	−34.02
A3-A7	−64.08	−4.44	4.13	−4.47	32.16	−51.85	−40.94	−25.00	5.56

Table A3. *Cont.*

Comparison	CO_{2e}	$SO_x + NO_x$	LCOE -2025	CO_{2e}	$SO_x + NO_x$	LCOE-2040 L	CO_{2e}	$SO_x + NO_x$	LCOE 2040 -H
A3-A8	−48.73	32.13	−13.48	−7.50	0.26	−41.99	−39.13	−2.12	1.45
A3-A9	−77.64	−3.13	4.09	−70.46	24.00	−6.66	−54.49	−21.18	4.83
A3-A10	−68.12	25.27	−9.56	−69.93	−2.35	−0.63	−53.66	−1.80	1.35
A3-A11	−105.29	−851.36	16.16	−97.29	−755.37	7.47	−100.15	−776.69	−7.90
A4-A5	54.86	0.73	−65.29	−57.85	32.83	−6.86	−7.07	0.26	−34.75
A4-A6	43.67	0.59	−58.66	−57.26	−3.11	1.25	−3.93	29.52	−40.34
A4-A7	−80.47	−57.44	16.91	−4.40	33.14	−52.80	−38.88	−2.10	1.44
A4-A8	−59.26	−3.64	−6.01	−7.52	0.27	−42.63	−37.05	20.98	−2.71
A4-A9	−90.23	−38.63	12.68	−72.04	24.59	−6.32	−53.00	−1.78	1.34
A4-A10	−78.12	−2.79	−3.44	−71.48	−2.40	−0.15	−52.17	17.77	−2.17
A4-A11	−113.76	−922.90	21.53	−98.63	−766.58	7.88	−99.62	−772.38	−10.98
A5-A6	−5.98	0.00	−29.28	−44.58	−781.22	N/F	N/F	N/F	−463.50
A5-A7	−126.99	−77.44	45.17	N/F	36.61	−568.53	−152.49	−10.53	N/F
A5-A8	−87.03	−4.71	8.42	N/F	−247.13	−314.36	−138.03	90.77	N/F
A5-A9	−120.37	−46.81	28.88	−114.42	0.00	−4.69	−142.12	−5.72	71.37
A5-A10	−101.54	−3.41	7.45	−110.15	−102.34	18.91	−137.06	50.72	59.15
A5-A11	−130.95	−1017.04	30.38	−131.70	−1414.73	19.84	−210.25	−1695.82	17.44
A6-A7	−137.15	−83.94	51.43	N/F	N/F	−1371.30	−171.62	−122.21	N/F
A6-A8	−91.74	−4.98	10.61	N/F	41.67	−580.05	−155.35	−9.52	N/F
A6-A9	−126.00	−49.11	31.74	−125.59	N/F	−33.75	−152.01	−64.92	85.43
A6-A10	−105.49	−3.55	8.97	−120.04	0.00	−4.92	−146.52	−5.21	72.47
A6-A11	−133.89	−1040.97	31.78	−135.09	−1439.38	13.72	−217.37	−1759.02	25.15

References

1. Sánchez, A.; Rengel, M.A.M.; Martín, M. Conceptual Design of a Large Ship Propulsion System Fueled by an Ammonia-Hydrogen Blend: Toward a Decarbonized Shipping Transport. In Proceedings of the 34th European Symposium on Computer Aided Process Engineering/15th International Symposium on Process Systems Engineering, Computer Aided Chemical Engineering, Florence, Italy, 2–6 June 2024; pp. 2143–2148.
2. Xiong, L.; Tian, L.; Zhang, X.; Lv, Y.; Zhang, H. Application of Microbial Technology for Enhancing Carbon Dioxide Geosequestration in Shallow Seabed Caprock. *J. Mar. Sci. Eng.* **2025**, *13*, 574. [CrossRef]
3. IMO. 2023 IMO Strategy on Reduction of GHG Emissions from Ships. Available online: https://www.imo.org/en/OurWork/Environment/Pages/2023-IMO-Strategy-on-Reduction-of-GHG-Emissions-from-Ships.aspx (accessed on 24 April 2024).
4. IMO. IMO's Work to Cut GHG Emissions from Ships. Available online: https://www.imo.org/en/MediaCentre/HotTopics/Pages/Cutting-GHG-emissions.aspx (accessed on 5 August 2024).
5. van Rheenen, E.S.; Padding, J.T.; Kana, A.A.; Visser, K. Comparative energy analysis of hydrogen carriers as energy source on ships. *J. Mar. Eng. Technol.* **2025**, 1–15. [CrossRef]
6. Van Rheenen, E.S.; Padding, J.T.; Slootweg, J.C.; Visser, K. Hydrogen carriers for zero-emission ship propulsion using PEM fuel cells: An evaluation. *J. Mar. Eng. Technol.* **2024**, *23*, 166–183. [CrossRef]
7. Rivard, E.; Trudeau, M.; Zaghib, K. Hydrogen Storage for Mobility: A Review. *Materials* **2019**, *12*, 1973. [CrossRef]
8. Aziz, M.; Wijayanta, A.T.; Nandiyanto, A.B.D. Ammonia as Effective Hydrogen Storage: A Review on Production, Storage and Utilization. *Energies* **2020**, *13*, 3062. [CrossRef]
9. Van Hoecke, L.; Laffineur, L.; Campe, R.; Perreault, P.; Verbruggen, S.W.; Lenaerts, S. Challenges in the use of hydrogen for maritime applications. *Energy Environ. Sci.* **2021**, *14*, 815–843. [CrossRef]
10. Zhang, M.; Li, M.; Wang, R.; Qian, Y. Effects of acute ammonia toxicity on oxidative stress, immune response and apoptosis of juvenile yellow catfish Pelteobagrus fulvidraco and the mitigation of exogenous taurine. *Fish Shellfish Immunol.* **2018**, *79*, 313–320. [CrossRef]
11. Braissant, O.; McLin, V.A.; Cudalbu, C. Ammonia toxicity to the brain. *J. Inherit. Metab. Dis.* **2013**, *36*, 595–612. [CrossRef]
12. Wang, Y.; Wright, L.A. A Comparative Review of Alternative Fuels for the Maritime Sector: Economic, Technology, and Policy Challenges for Clean Energy Implementation. *World* **2021**, *2*, 456–481. [CrossRef]
13. Duong, P.A.; Jinuk, L.; Rim, R.B.; Kang, H. A preliminary safety assessment of fuel gas supply system in the engine room of the ammonia fuelled ship. *J. Mar. Eng. Technol.* **2025**, 1–20. [CrossRef]
14. Chavando, A.; Silva, V.; Cardoso, J.; Eusebio, D. Advancements and Challenges of Ammonia as a Sustainable Fuel for the Maritime Industry. *Energies* **2024**, *17*, 3183. [CrossRef]
15. Andriani, D.; Bicer, Y. A Review of Hydrogen Production from Onboard Ammonia Decomposition: Maritime Applications of Concentrated Solar Energy and Boil-Off Gas Recovery. *Fuel* **2023**, *352*, 128900. [CrossRef]
16. Boggs, B.K.; Botte, G.G. On-board hydrogen storage and production: An application of ammonia electrolysis. *J. Power Sources* **2009**, *192*, 573–581. [CrossRef]
17. Wang, W.; Herreros, J.M.; Tsolakis, A.; York, A.P.E. Ammonia as hydrogen carrier for transportation; Investigation of the ammonia exhaust gas fuel reforming. *Int. J. Hydrogen Energy* **2013**, *38*, 9907–9917. [CrossRef]
18. McKinlay, C.J.; Manias, P.; Turnock, S.R.; Hudson, D.A. Dynamic Modelling of Ammonia Crackers and Hydrogen Pem Fuel Cells for Shipping Applications. In Proceedings of the International Conference on Computer Applications in Shipbuilding)(ICCAS) 2022, Yokohama, Japan, 13–15 September 2022.
19. Ye, M.; Sharp, P.; Brandon, N.; Kucernak, A. System-level comparison of ammonia, compressed and liquid hydrogen as fuels for polymer electrolyte fuel cell powered shipping. *Int. J. Hydrogen Energy* **2022**, *47*, 8565–8584. [CrossRef]
20. Zhu, R.; Wang, Z.; He, Y.; Zhu, Y.; Cen, K. LCA comparison analysis for two types of H2 carriers: Methanol and ammonia. *Int. J. Energy Res.* **2022**, *46*, 11818–11833. [CrossRef]
21. Spatolisano, E.; Pellegrini, L.A.; de Angelis, A.R.; Cattaneo, S.; Roccaro, E. Ammonia as a Carbon-Free Energy Carrier: NH_3 Cracking to H_2. *Ind. Eng. Chem. Res.* **2023**, *62*, 10813–10827. [CrossRef]
22. Duong, P.A.; Ryu, B.R.; Lee, H.Y.Y.; Kang, H.K. Thermodynamic analysis of integrated ammonia fuel cells system for maritime application. *Energy Rep.* **2023**, *10*, 1521–1537. [CrossRef]
23. Restelli, F.; Spatolisano, E.; Pellegrini, L.A.; de Angelis, A.R.; Cattaneo, S.; Roccaro, E. Detailed techno-economic assessment of ammonia as green H_2 carrier. *Int. J. Hydrogen Energy* **2024**, *52*, 532–547. [CrossRef]
24. Di Micco, S.; Cigolotti, V.; Mastropasqua, L.; Brouwer, J.; Minutillo, M. Ammonia-powered ships: Concept design and feasibility assessment of powertrain systems for a sustainable approach in maritime industry. *Energy Convers. Manag. X* **2024**, *22*, 100539. [CrossRef]
25. Duong, P.A.; Ryu, B.R.; Lee, J.; Kang, H. Techno-Economic Analysis of a Direct Ammonia Solid Oxide Fuel Cell–Integrated System for Marine Vessels. *Chem. Eng. Technol.* **2025**, *48*, e12013. [CrossRef]

26. Sarı, A.; Sulukan, E.; Özkan, D.; Sıdkı Uyar, T. Environmental impact assessment of hydrogen-based auxiliary power system onboard. *Int. J. Hydrogen Energy* **2021**, *46*, 29680–29693. [CrossRef]
27. Vieira, G.T.T.; Pereira, D.F.; Taheri, S.I.; Khan, K.S.; Salles, M.B.C.; Guerrero, J.M.; Carmo, B.S. Optimized Configuration of Diesel Engine-Fuel Cell-Battery Hybrid Power Systems in a Platform Supply Vessel to Reduce CO_2 Emissions. *Energies* **2022**, *15*, 2184. [CrossRef]
28. Bang, E.-S.; Kim, M.-H.; Park, S.-K. Options for Methane Fuel Processing in PEMFC System with Potential Maritime Applications. *Energies* **2022**, *15*, 8604. [CrossRef]
29. Bagherabadi, K.M.; Skjong, S.; Bruinsma, J.; Pedersen, E. System-level modeling of marine power plant with PEMFC system and battery. *Int. J. Nav. Archit. Ocean Eng.* **2022**, *14*, 100487. [CrossRef]
30. Lee, H.; Ryu, B.; Anh, D.P.; Roh, G.; Lee, S.; Kang, H. Thermodynamic analysis and assessment of novel ORC- DEC integrated PEMFC system for liquid hydrogen fueled ship application. *Int. J. Hydrogen Energy* **2023**, *48*, 3135–3153. [CrossRef]
31. Wang, Z.; Dong, B.; Wang, Y.; Li, M.; Liu, H.; Han, F. Analysis and evaluation of fuel cell technologies for sustainable ship power: Energy efficiency and environmental impact. *Energy Convers. Manag. X* **2024**, *21*, 100482. [CrossRef]
32. Penga, J.; Vidović, T.; Radica, G.; Penga, Ž. Analysis of Hybrid Ship Machinery System with Proton Exchange Membrane Fuel Cells and Battery Pack. *Appl. Sci.* **2024**, *14*, 2878. [CrossRef]
33. Yuksel, O.; Blanco-Davis, E.; Spiteri, A.; Hitchmough, D.; Shagar, V.; Di Piazza, M.C.; Pucci, M.; Tsoulakos, N.; Armin, M.; Wang, J. Optimising the Design of a Hybrid Fuel Cell/Battery and Waste Heat Recovery System for Retrofitting Ship Power Generation. *Energies* **2025**, *18*, 288. [CrossRef]
34. Aziz, M.; Trinh, P.-H.; Hudaya, C.; Chung, I.-Y. Coordinated control strategy for hybrid multi-PEMFC/BESS in a shipboard power system. *Electr. Power Syst. Res.* **2025**, *243*, 111495. [CrossRef]
35. LAROS. How Laros Works? Available online: https://www.laros.gr/ (accessed on 20 December 2024).
36. PowerCellGroup. Marine System 200. Available online: https://powercellgroup.com/product/marine-system-200/ (accessed on 1 May 2024).
37. Yuksel, O.; Koseoglu, B. Numerical simulation of the hybrid ship power distribution system and an analysis of its emission reduction potential. *Ships Offshore Struct.* **2023**, *18*, 78–94. [CrossRef]
38. Ristig, S.; Poschmann, M.; Folke, J.; Gómez-Cápiro, O.; Chen, Z.; Sanchez-Bastardo, N.; Schlögl, R.; Heumann, S.; Ruland, H. Ammonia Decomposition in the Process Chain for a Renewable Hydrogen Supply. *Chem. Ing. Tech.* **2022**, *94*, 1413–1425. [CrossRef]
39. Cha, J.; Park, Y.; Brigljević, B.; Lee, B.; Lim, D.; Lee, T.; Jeong, H.; Kim, Y.; Sohn, H.; Mikulčić, H.; et al. An efficient process for sustainable and scalable hydrogen production from green ammonia. *Renew. Sustain. Energy Rev.* **2021**, *152*, 111562. [CrossRef]
40. Xu, Y.-F.; Duchesne, P.N.; Wang, L.; Tavasoli, A.; Ali, F.M.; Xia, M.; Liao, J.-F.; Kuang, D.-B.; Ozin, G.A. High-performance light-driven heterogeneous CO(2) catalysis with near-unity selectivity on metal phosphides. *Nat. Commun.* **2020**, *11*, 5149. [CrossRef]
41. Devkota, S.; Shin, B.-J.; Mun, J.-H.; Kang, T.-H.; Yoon, H.C.; Mazari, S.A.; Moon, J.-H. Process design and optimization of onsite hydrogen production from ammonia: Reactor design, energy saving and NOX control. *Fuel* **2023**, *342*, 127879. [CrossRef]
42. Crystec. Ammonia Cracker for the Generation of Forming Gas. Available online: https://www.crystec.com/kllhyame.htm#Hydrogen_PSA (accessed on 7 August 2024).
43. Nami, H.; Hendriksen, P.V.; Frandsen, H.L. Green ammonia production using current and emerging electrolysis technologies. *Renew. Sustain. Energy Rev.* **2024**, *199*, 114517. [CrossRef]
44. Ochoa, N. Comparative Life Cycle Assessment of Ammonia Production Pathways. Master's Thesis, Aalto University, Espoo, Finland, 2023.
45. Hatzell, M.C. The Colors of Ammonia. *ACS Energy Lett.* **2024**, *9*, 2920–2921. [CrossRef]
46. Lee, K.; Liu, X.; Vyawahare, P.; Sun, P.; Elgowainy, A.; Wang, M. Techno-economic performances and life cycle greenhouse gas emissions of various ammonia production pathways including conventional, carbon-capturing, nuclear-powered, and renewable production. *Green Chem.* **2022**, *24*, 4830–4844. [CrossRef]
47. Rambert, O.; Febvre, L. The Challenges of Hydrogen Storage on a Large Scale. Available online: https://hysafe.info/uploads/papers/2021/189.pdf (accessed on 21 June 2024).
48. Raucci, C.; Calleya, J.; Suarez De La Fuente, S.; Pawling, R. Hydrogen on Board Ship: A First Analysis of Key Parameters and Implications. Available online: https://decarbonisingfreight.co.uk/wp-content/uploads/2023/05/Raucci-et-al-2015-Hydrogen-on-board-ship.pdf (accessed on 21 June 2024).
49. Panasonic. Specifications for NCR18650GA. Available online: https://www.orbtronic.com/content/Datasheet-specs-Sanyo-Panasonic-NCR18650GA-3500mah.pdf (accessed on 1 May 2024).
50. Saxena, S.; Hendricks, C.; Pecht, M. Cycle life testing and modeling of graphite/LiCoO2 cells under different state of charge ranges. *J. Power Sources* **2016**, *327*, 394–400. [CrossRef]

51. Sepasi, S.; Ghorbani, R.; Liaw, B.Y. Inline state of health estimation of lithium-ion batteries using state of charge calculation. *J. Power Sources* **2015**, *299*, 246–254. [CrossRef]
52. SMA. Sunny Central Storage. Available online: https://files.sma.de/assets/275864.pdf (accessed on 23 May 2024).
53. Konur, O.; Yuksel, O.; Aykut Korkmaz, S.; Ozgur Colpan, C.; Saatcioglu, O.Y.; Koseoglu, B. Operation-dependent exergetic sustainability assessment and environmental analysis on a large tanker ship utilizing Organic Rankine cycle system. *Energy* **2023**, *262*, 125477. [CrossRef]
54. Konur, O.; Yuksel, O.; Korkmaz, S.A.; Colpan, C.O.; Saatcioglu, O.Y.; Muslu, I. Thermal design and analysis of an organic rankine cycle system utilizing the main engine and cargo oil pump turbine based waste heats in a large tanker ship. *J. Clean. Prod.* **2022**, *368*, 133230. [CrossRef]
55. Konur, O.; Saatcioglu, O.Y.; Korkmaz, S.A.; Erdogan, A.; Colpan, C.O. Heat exchanger network design of an organic Rankine cycle integrated waste heat recovery system of a marine vessel using pinch point analysis. *Int. J. Energy Res.* **2020**, *44*, 12312–12328. [CrossRef]
56. Lyu, L.; Kan, A.; Chen, W.; Zhang, Y.; Fu, B. Energy, Exergy and Environmental Analysis of ORC Waste Heat Recovery from Container Ship Exhaust Gases Based on Voyage Cycle. *J. Mar. Sci. Eng.* **2023**, *11*, 2029. [CrossRef]
57. Gilbert, P.; Walsh, C.; Traut, M.; Kesieme, U.; Pazouki, K.; Murphy, A. Assessment of full life-cycle air emissions of alternative shipping fuels. *J. Clean. Prod.* **2018**, *172*, 855–866. [CrossRef]
58. Yuksel, O. A comprehensive feasibility analysis of dual-fuel engines and solid oxide fuel cells on a tanker ship considering environmental, economic, and regulation aspects. *Sustain. Prod. Consum.* **2023**, *42*, 106–124. [CrossRef]
59. Pavlenko, N.; Comer, B.; Zhou, Y.; Clark, N. *The Climate Implications of Using LNG as A Marine Fuel*; International Council on Clean Transportation: Washington, DC, USA, 2020.
60. Kuzu, S.L.; Bilgili, L.; Kiliç, A. Estimation and dispersion analysis of shipping emissions in Bandirma Port, Turkey. *Environ. Dev. Sustain.* **2021**, *23*, 10288–10308. [CrossRef]
61. Dulău, L.-I. CO2 Emissions of Battery Electric Vehicles and Hydrogen Fuel Cell Vehicles. *Clean Technol.* **2023**, *5*, 696–712. [CrossRef]
62. IMO. 2024 Guidelines on Life Cycle Ghg Intensity of Marine Fuels (2024 LCA Guidelines). Available online: https://wwwcdn.imo.org/localresources/en/KnowledgeCentre/IndexofIMOResolutions/MEPCDocuments/MEPC.391(81).pdf (accessed on 13 November 2024).
63. Shen, W.; Chen, X.; Qiu, J.; Hayward, J.A.; Sayeef, S.; Osman, P.; Meng, K.; Dong, Z.Y. A comprehensive review of variable renewable energy levelized cost of electricity. *Renew. Sustain. Energy Rev.* **2020**, *133*, 110301. [CrossRef]
64. IEA. Projected Costs of Generating Electricity. Available online: https://www.oecd-nea.org/upload/docs/application/pdf/2020-12/egc-2020_2020-12-09_18-26-46_781.pdf (accessed on 27 June 2024).
65. Hansen, K. Decision-making based on energy costs: Comparing levelized cost of energy and energy system costs. *Energy Strategy Rev.* **2019**, *24*, 68–82. [CrossRef]
66. Shu, G.; Liu, P.; Tian, H.; Wang, X.; Jing, D. Operational profile based thermal-economic analysis on an Organic Rankine cycle using for harvesting marine engine's exhaust waste heat. *Energy Convers. Manag.* **2017**, *146*, 107–123. [CrossRef]
67. Gianni, M.; Pietra, A.; Taccani, R. Outlook of future implementation of PEMFC and SOFC onboard cruise ships. In Proceedings of the E3S Web of Conferences, 100RES 2020—Applied Energy Symposium (ICAE), Pisa, Italy, 25–30 October 2020; 2021.
68. Wang, Y.; Pang, Y.; Xu, H.; Martinez, A.; Chen, K.S. PEM Fuel cell and electrolysis cell technologies and hydrogen infrastructure development—A review. *Energy Environ. Sci.* **2022**, *15*, 2288–2328. [CrossRef]
69. Ammar, N.R.; Seddiek, I.S. Hybrid/dual fuel propulsion systems towards decarbonization: Case study container ship. *Ocean Eng.* **2023**, *281*, 114962. [CrossRef]
70. Seo, Y.; Han, S. Economic Evaluation of an Ammonia-Fueled Ammonia Carrier Depending on Methods of Ammonia Fuel Storage. *Energies* **2021**, *14*, 8326. [CrossRef]
71. Jackson, C.; Fothergill, K.; Gray, P.; Haroon, F.; Makhloufi, C.; Kezibri, N.; Davey, A.; LHote, O.; Zarea, M.; Davenne, T.; et al. Ammonia to Green Hydrogen Project. 2020. Available online: https://assets.publishing.service.gov.uk/media/5ea1705fd3bf7f7b4cadb7c5/HS420_-_Ecuity_-_Ammonia_to_Green_Hydrogen.pdf (accessed on 25 April 2025).
72. Richard, S.; Ramirez Santos, A.; Olivier, P.; Gallucci, F. Techno-economic analysis of ammonia cracking for large scale power generation. *Int. J. Hydrogen Energy* **2024**, *71*, 571–587. [CrossRef]
73. Terlouw, T.; Bauer, C.; McKenna, R.; Mazzotti, M. Large-scale hydrogen production via water electrolysis: A techno-economic and environmental assessment. *Energy Environ. Sci.* **2022**, *15*, 3583–3602. [CrossRef]
74. Korkmaz, S.A.; Erginer, K.E.; Yuksel, O.; Konur, O.; Colpan, C.O. Environmental and economic analyses of fuel cell and battery-based hybrid systems utilized as auxiliary power units on a chemical tanker vessel. *Int. J. Hydrogen Energy* **2023**, *48*, 23279–23295. [CrossRef]
75. Maxwell, C. Cost Indices. Available online: https://toweringskills.com/financial-analysis/cost-indices/ (accessed on 25 June 2024).

76. Cesaro, Z.; Ives, M.; Nayak-Luke, R.; Mason, M.; Bañares-Alcántara, R. Ammonia to power: Forecasting the levelized cost of electricity from green ammonia in large-scale power plants. *Appl. Energy* **2021**, *282*, 116009. [CrossRef]
77. Navarrete, A.; Zhou, Y. The Price of Green Hydrogen: How and Why We Estimate Future Production Costs. Available online: https://theicct.org/the-price-of-green-hydrogen-estimate-future-production-costs-may24/ (accessed on 14 August 2024).
78. Helgason, R.; Cook, D.; Davíðsdóttir, B. An evaluation of the cost-competitiveness of maritime fuels—A comparison of heavy fuel oil and methanol (renewable and natural gas) in Iceland. *Sustain. Prod. Consum.* **2020**, *23*, 236–248. [CrossRef]
79. ShipandBunker. World Bunker Prices. Available online: https://shipandbunker.com/prices (accessed on 25 June 2024).
80. Zou, J.; Yang, B. Evaluation of alternative marine fuels from dual perspectives considering multiple vessel sizes. *Transp. Res. Part D Transp. Environ.* **2023**, *115*, 103583. [CrossRef]
81. Taherdoost, H.; Mohebi, A. A Comprehensive Guide to the COPRAS method for Multi-Criteria Decision Making. *J. Manag. Sci. Eng. Res.* **2024**, *7*, 1–14. [CrossRef]
82. Zavadskas, E.K.; Kaklauskas, A.; Vilutienė, T. Multicriteria Evaluation of Apartment Blocks Maintenance Contractors: Lithuanian Case Study. *Int. J. Strateg. Prop. Manag.* **2009**, *13*, 319–338. [CrossRef]
83. Podvezko, V. The Comparative Analysis of MCDA Methods SAW and COPRAS. *Eng. Econ.* **2011**, *22*, 134–146. [CrossRef]
84. Zavadskas, E.K.; Turskis, Z.; Kildienė, S. State of Art Surveys of Overviews on Mcdm/Madm Methods. *Technol. Econ. Dev. Econ.* **2014**, *20*, 165–179. [CrossRef]
85. Ghorabaee, M.K.; Amiri, M.; Zavadskas, E.K.; Turskis, Z. Multi-criteria group decision-making using an extended edas method with interval type-2 fuzzy sets. *E+M Ekon. A Manag.* **2017**, *20*, 48–68. [CrossRef]
86. Shannon, C.E. A mathematical theory of communication. *Bell Syst. Tech. J.* **1948**, *27*, 379–423. [CrossRef]
87. Zou, Z.-h.; Yun, Y.; Sun, J.-n. Entropy method for determination of weight of evaluating indicators in fuzzy synthetic evaluation for water quality assessment. *J. Environ. Sci.* **2006**, *18*, 1020–1023. [CrossRef]
88. Sagiroglu, A.; Caliskan Demir, M.; Taskin, A. Assessing collaboration performance of NGOs by a decomposed Fuzzy approach utilizing AHP and COPRAS methods: Turkiye case. *Int. J. Disaster Risk Reduct.* **2024**, *111*, 104744. [CrossRef]
89. Kumar, R.; Kumar, S.; Ağbulut, Ü.; Gürel, A.E.; Alwetaishi, M.; Shaik, S.; Saleel, C.A.; Lee, D. Parametric optimization of an impingement jet solar air heater for active green heating in buildings using hybrid CRITIC-COPRAS approach. *Int. J. Therm. Sci.* **2024**, *197*, 108760. [CrossRef]
90. Triantaphyllou, E.; Sánchez, A. A Sensitivity Analysis Approach for Some Deterministic Multi-Criteria Decision-Making Methods. *Decis. Sci.* **1997**, *28*, 151–194. [CrossRef]
91. Esen, H.; Inalli, M.; Esen, M.; Pihtili, K. Energy and exergy analysis of a ground-coupled heat pump system with two horizontal ground heat exchangers. *Build. Environ.* **2007**, *42*, 3606–3615. [CrossRef]
92. Taner, T.; Sivrioglu, M. Energy–exergy analysis and optimisation of a model sugar factory in Turkey. *Energy* **2015**, *93*, 641–654. [CrossRef]
93. Taner, T. Optimisation processes of energy efficiency for a drying plant: A case of study for Turkey. *Appl. Therm. Eng.* **2015**, *80*, 247–260. [CrossRef]
94. Akpinar, E.K. Mathematical modelling of thin layer drying process under open sun of some aromatic plants. *J. Food Eng.* **2006**, *77*, 864–870. [CrossRef]
95. Issa, M.; Ilinca, A.; Martini, F. Ship Energy Efficiency and Maritime Sector Initiatives to Reduce Carbon Emissions. *Energies* **2022**, *15*, 7910. [CrossRef]
96. Alzayedi, A.M.T.; Alkhaledi, A.N.F.N.R.; Sampath, S.; Pilidis, P. TERA of Gas Turbine Propulsion Systems for RORO Ships. *Energies* **2023**, *16*, 5875. [CrossRef]
97. Snustad, I.; Berstad, D.; Nekså, P. Hydrogen bunkering from a fuel island onto fishing vessels. *Int. J. Hydrogen Energy* **2024**, *92*, 1248–1255. [CrossRef]
98. Panić, I.; Cuculić, A.; Ćelić, J. Color-Coded Hydrogen: Production and Storage in Maritime Sector. *J. Mar. Sci. Eng.* **2022**, *10*, 1995. [CrossRef]
99. van Biert, L.; Godjevac, M.; Visser, K.; Aravind, P.V. A review of fuel cell systems for maritime applications. *J. Power Sources* **2016**, *327*, 345–364. [CrossRef]
100. Bicer, Y.; Dincer, I.; Vezina, G.; Raso, F. Impact Assessment and Environmental Evaluation of Various Ammonia Production Processes. *Environ. Manag.* **2017**, *59*, 842–855. [CrossRef]
101. Bicer, Y.; Dincer, I. Life cycle assessment of nuclear-based hydrogen and ammonia production options: A comparative evaluation. *Int. J. Hydrogen Energy* **2017**, *42*, 21559–21570. [CrossRef]
102. Bayraktar, M.; Yüksel, O. Analysis of the nuclear energy systems as an alternative propulsion system option on commercial marine vessels by utilizing the SWOT-AHP method. *Nucl. Eng. Des.* **2023**, *407*, 112265. [CrossRef]
103. Brook, B.W.; Bradshaw, C.J.A. Key role for nuclear energy in global biodiversity conservation. *Conserv. Biol.* **2015**, *29*, 702–712. [CrossRef]

104. Lenzen, M. Life cycle energy and greenhouse gas emissions of nuclear energy: A review. *Energy Convers. Manag.* **2008**, *49*, 2178–2199. [CrossRef]
105. Jin, T.; Kim, J. What is better for mitigating carbon emissions—Renewable energy or nuclear energy? A panel data analysis. *Renew. Sustain. Energy Rev.* **2018**, *91*, 464–471. [CrossRef]
106. Yuksel, O.; Bayraktar, M.; Seyhan, A. Environmental and economic analysis of cold ironing using renewable hybrid systems. In *Clean Technologies and Environmental Policy*; Springer Nature: Berlin, Germany, 2024. [CrossRef]
107. Capros, P.; Zazias, G.; Evangelopoulou, S.; Kannavou, M.; Fotiou, T.; Siskos, P.; De Vita, A.; Sakellaris, K. Energy-system modelling of the EU strategy towards climate-neutrality. *Energy Policy* **2019**, *134*, 110960. [CrossRef]
108. Bayraktar, M. Investigation of alternative fuelled marine diesel engines and waste heat recovery system utilization on the oil tanker for upcoming regulations and carbon tax. *Ocean Eng.* **2023**, *287*, 115831. [CrossRef]
109. Masia, B.; Yang, M.; Cozzani, V. Risk Assessment of Ammonia Fueled Ships: Consequences on Human Health of Ammonia Releases from Damaged Fuel Storage Tanks. *ACS Chem. Health Saf.* **2024**, *31*, 503–520. [CrossRef]
110. Furstenberg Stott, C. The NH3 Kraken: Amogy's Ammonia-Powered Tugboat. Available online: https://ammoniaenergy.org/articles/the-nh3-kraken-amogys-ammonia-powered-tugboat/?utm_source=chatgpt.com (accessed on 29 April 2025).
111. Mcdermott, J.; Hill, M. Tugboat Powered by Ammonia Sails for the First Time, Showing How to Cut Emissions from Shipping. Available online: https://apnews.com/article/ammonia-fuel-diesel-amogy-shipping-60beccfb8894c79ddc624026fbf0a8e5 (accessed on 29 April 2025).